Available online at www.sciencedirect.com
ScienceDirect
Geochimica et Cosmochimica Acta 71 (2007) 2609–2636
Geochimica et Cosmochimica Acta
www.elsevier.com/locate/gca

# Early Cretaceous adakitic granites in the Northern Dabie Complex, central China: Implications for partial melting and delamination of thickened lower crust

Qiang Wang [a,*], Derek A. Wyman [b], Jifeng Xu [a], Ping Jian [c], Zhenhua Zhao [a], Chaofeng Li [d], Wei Xu [e], Jinlong Ma [a], Bin He [a]

[a] *Key Laboratory of Isotope Geochronology and Geochemistry, Guangzhou Institute of Geochemistry, Chinese Academy of Sciences, Guangzhou 510640, PR China*
[b] *School of Geosciences, Division of Geology and Geophysics, The University of Sydney, NSW 2006, Australia*
[c] *Chinese Academy of Geological Science, 26 Beiwanzhuang Road, Beijing 100037, PR China*
[d] *Institute of Geology and Geophysics, Chinese Academy of Sciences, Beijing 100029, PR China*
[e] *Academy of Geological Survey of Anhui Province, Ningguo Road 19, Hefei 230001, PR China*

Received 3 July 2006; accepted in revised form 14 March 2007; available online 24 March 2007

**Abstract**

To date, few adakitic rocks have been reported in direct association with contemporary intra-continental extensional structures, which has cast doubt on genetic models involving partial melting of the lower crust. This study presents Early Cretaceous (143–129 Ma, new Sensitive high-resolution ion microprobe (SHRIMP) zircon U-Pb ages) adakitic granites, which are directly associated with a contemporary metamorphic core complex (i.e., the Northern Dabie Complex in the Dabie area). These granites exhibit relatively high Sr contents, negligible to positive Eu and Sr anomalies, high La/Yb and Sr/Y ratios, but very low Yb and Y contents, similar to subducted oceanic crust-derived adakites. They are also characterized, however, by very low MgO or $Mg^{\#}$ and Ni values, and Nd–Sr isotope compositions ($\varepsilon_{Nd}(t) = -14.6$ to $-19.4$ and $(^{87}Sr/^{86}Sr)_i = 0.7067$–$0.7087$) similar to Triassic continent-derived eclogites subducted in the Dabie–Sulu Orogen. Additionally, late granitic dikes in the adakitic intrusions exhibit low Sr contents, clearly negative Eu and Sr anomalies, low La/Yb and Sr/Y ratios, but relatively high Yb and Y contents, similar to 118–105 Ma granites in the Northern Dabie Complex. Based on composition and geochronology data of Neoproterozoic amphibolites and orthogneisses, Triassic high- to ultra-high pressure metamorphic rocks, and Early Cretaceous mafic–ultramafic intrusive rocks, and the constraints provided by experimental melt data for tonalites, metabasaltic rocks and eclogites, we suggest that the adakitic granites were most probably generated by partial melting of thickened amphibole or rutile-bearing eclogitic lower crust as a consequence of Triassic–Middle Jurassic subduction and thrusting. The late dikes probably originated from plagioclase-bearing intermediate granulites. Moreover, we suggest that late Mesozoic delamination or foundering of thickened eclogitic lower crust is also a more plausible mechanism for the petrogenesis of Early Cretaceous mafic–ultramafic intrusive rocks in the Dabie area, and probably involved partial melting of a mixed source comprising eclogitic lower crust that had delaminated or foundered into upper lithospheric or asthenospheric mantle peridotite. Asthenospheric upwelling in response to post-collisional delamination of lithospheric mantle was likely to have provided the heat source for the Cretaceous magmatism.


## 1. INTRODUCTION

Since Defant and Drummond (1990) first distinguished adakites in Cenozoic arcs on the basis of their distinctive geochemical characteristics (e.g., high Sr, Sr/Y and La/Yb

* Corresponding author. Fax: +86 20 85290130.
*E-mail address:* wqiang@gig.ac.cn (Q. Wang).

0016-7037/$ - see front matter © 2007 Elsevier Ltd. All rights reserved.
doi:10.1016/j.gca.2007.03.008

values and low Y and Yb contents), these rocks have frequently been cited as possible examples of partial melts of subducted oceanic crust (e.g., Kay et al., 1993; Stern and Kilian, 1996; Smithies and Champion, 2000; Martin et al., 2005). It has also been suggested, however, that some Cenozoic adakitic rocks may be derived by partial melting of thickened lower crust (e.g., Atherton and Petford, 1993; Petford and Atherton, 1996; Topuz et al., 2005; Castillo, 2006) or by assimilation and fractional crystallization (AFC) processes acting on parental basaltic magmas, in an arc setting (e.g., Castillo et al., 1999).

In theory, intra-continental occurrences of adakitic rocks should be less contentious examples of granitic magmas generated by partial melting of thickened or delaminated lower crust (e.g., Zhang et al., 2001; Rapp et al., 2002; Xu et al., 2002; Chung et al., 2003; Gao et al., 2004; Wang et al., 2005a, 2006a,b). None of these examples of lower crust-derived adakitic rocks are directly associated with contemporary intra-continental extensional structures, however, and their tectonic setting therefore remains ambiguous. Given the uncertainties in the tectonic settings of these earlier studies, occurrences of post-collisional Cretaceous adakitic rocks of the Dabie area may provide a unique test case for non-subduction genetic models. The area is dominated by the Hong'an–Dabie–Sulu ultrahigh-pressure (UHP) metamorphic belt, which is the largest among seven recognized UHP belts in the world (Hacker et al., 1996) and was formed by Triassic collision between the North China and Yangtze Blocks (e.g., Zhai and Cong, 1996; Rowley et al., 1997; Hacker et al., 1998, 2000, 2004; Li et al., 2000; Ayers et al., 2002; Sun et al., 2002; Liu et al., 2004, 2006; Wan et al., 2005). The discovery of UHP minerals (coesite and diamond) (e.g., Xu et al., 2003 and references therein) and the texture of pyroxene exsolution from garnet (Ye et al., 2000) in the UHP metamorphic rocks indicated that continental crust was deeply subducted to >120–200 km and then rapidly exhumed from mantle depths back to crustal levels. Although some degree of melting has taken place during the subduction and subsequent exhumation of continental crust in some other UHP metamorphic belts (e.g., Hermann et al., 2001), the lack of Triassic and Jurassic granites or any orogenic magmatism (e.g., Tsai et al., 2000) suggests that significant syn-collisional or subsequent (during exhumation) partial melting of subducted continent did not take place in the Dabie UHP metamorphic belt. In contrast, Cretaceous intrusive and volcanic rocks comprising 47% of the surface exposure of the Dabie Orogen (e.g., Ratschbacher et al., 2000) indicate that post-collisional melting occurred widely in the area. Apart from occurrences of Neoproterozoic metamorphic rocks in the area (Bryant et al., 2004), the Northern Dabie Complex mainly consists of these Cretaceous granite intrusions (Hacker et al., 1998; Ratschbacher et al., 2000; Bryant et al., 2004). Detailed structural studies and geochronological data indicated that the Northern Dabie Complex is an asymmetric structural dome (i.e., metamorphic core complex) that formed during Cretaceous NW–SE sub-horizontal extension (Hacker et al., 1998, 2004; Ratschbacher et al., 2000).

Our recent investigation indicates that adakitic rocks occur in the Northern Dabie Complex (Wang et al., 2001). Here, new sensitive high-resolution ion microprobe (SHRIMP) zircon geochronology data show that the adakitic rocks were intruded in the Early Cretaceous (143–129 Ma). These Early Cretaceous adakitic granites not only provide important evidence for the post-collisional evolution of the Dabie Orogen, but also represent the first case of adakitic rocks that are directly associated with an intra-continental extensional metamorphic core complex. Accordingly, they represent an important case study for models of adakite genesis from thickened lower continental crust.

## 2. GEOLOGICAL BACKGROUND

The Dabie ultrahigh-pressure (UHP) metamorphic belt is part of the 2000 km long Qinling–Hong'an–Dabie–Sulu Orogen and formed by subduction of the Yangtze Block beneath the Northern China Block in the Triassic (Fig. 1a) (e.g., Ratschbacher et al., 2003; Hacker et al., 2004).The Dabie Orogen can be divided, from north to south, into the North Huaiyang (NHY), the Northern Dabie Complex (NDC), and the UHP–HP (high-pressure) metamorphic units (e.g., Zhai and Cong, 1996; Hacker et al., 1998; Ratschbacher et al., 2000).

The NHY unit, which is located between the Triassic suture to the north and Xiaotian–Mozitan fault to the south (Fig. 1b), consists of greenshist-facies metamorphic rocks of the Foziling and Luzhengguan Groups. Their protoliths have zircon ages of 700–800 Ma (Hacker et al., 1998, 2000; Chen et al., 2003), suggesting that the NHY unit was a part of the Yangtze Block rather than the Northern China Block (NCB) because it contains ~770 Ma zircons whereas the southern margin of the NCB is characterized by ~400 and 480 Ma zircons (Hacker et al., 1998, 2000).

The NDC unit is bounded by the Xiaotian–Mozitan fault to the north, the Wuhe–Shuihou fault to the south, the Shang–Ma fault to the west and the Tan–Lu fault to the east (Fig. 1b). In addition to large-scale Cretaceous

Fig. 1. (a) The Mesozoic Qinling–Tongbai–Hong'an–Dabie–Sulu collisional orogen in eastern China (after Ratschbacher et al., 2003; Hacker et al., 2004). Cretaceous granites from Gilder et al. (1999), Li (2000) and Cretaceous A-type granites from Wang et al. (2000b, 2005b), Xie et al. (2004) and references therein. (b) Geological map of the Dabie and Hong'an area (after Hacker et al., 1998, 2000, 2004). Eclogite locations in the Northern Dabie Complex are from Xu et al. (2003), Hacker et al. (2004), Liu et al. (2005). Other eclogite locations are after Hacker et al. (2000, 2004) and references therein. Geochronology data for Cretaceous granites and mafic–ultramafic intrusive rocks are from Li and Wang (1991), Xue et al. (1997), Hacker et al. (1998), Ma et al. (1998), Wang et al. (1998), Jahn et al. (1999), Li et al. (1999), Wang and Deng (2002), Zhang et al. (2002a), Bryant et al. (2004), Xie et al. (2004), Zhao et al. (2005), and this study. Age data: Z, zircon U–Pb ages; R, whole rock and mineral Rb–Sr isochronal ages; HA, hornblende $^{40}Ar$–$^{39}Ar$ ages; BA, biotite $^{40}Ar$–$^{39}Ar$ ages; FKA–feldspar K–Ar ages. (c) Geological map of the Jiuzihe–Zhangjiazui area.

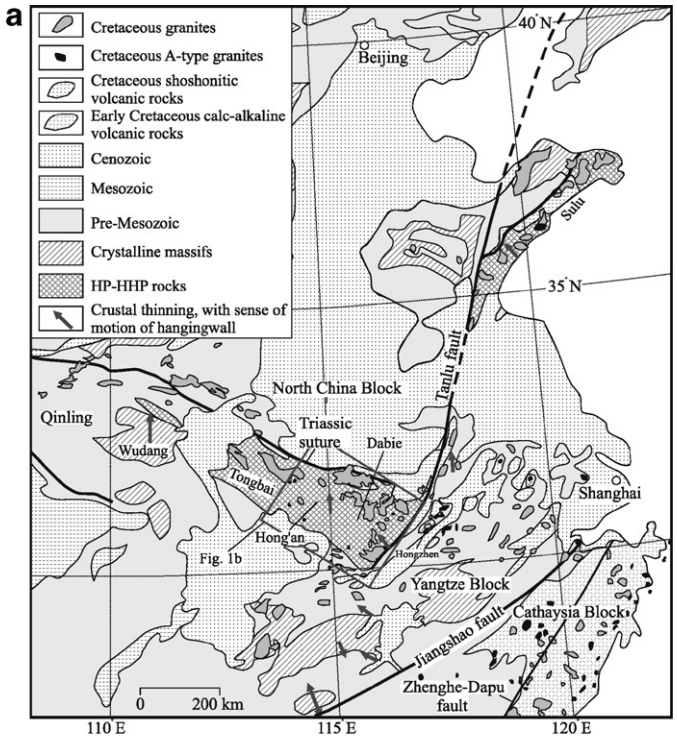
a
Cretaceous granites
Cretaceous A-type granites
Cretaceous shoshonitic volcanic rocks
Early Cretaceous calc-alkaline volcanic rocks
Cenozoic
Mesozoic
Pre-Mesozoic
Crystalline massifs
HP-HHP rocks
Crustal thinning, with sense of motion of hangingwall
Beijing
40°N
35°N
Sulu
Tanlu fault
North China Block
Qinling
Triassic suture
Dabie
Wudang
Tongbai
Hong'an
Fig. 1b
Hongzhen
Shanghai
Yangtze Block
Cathaysia Block
Jiangshao fault
Zhenghe-Dapu fault
0 200 km
110°E
115°E
120°E

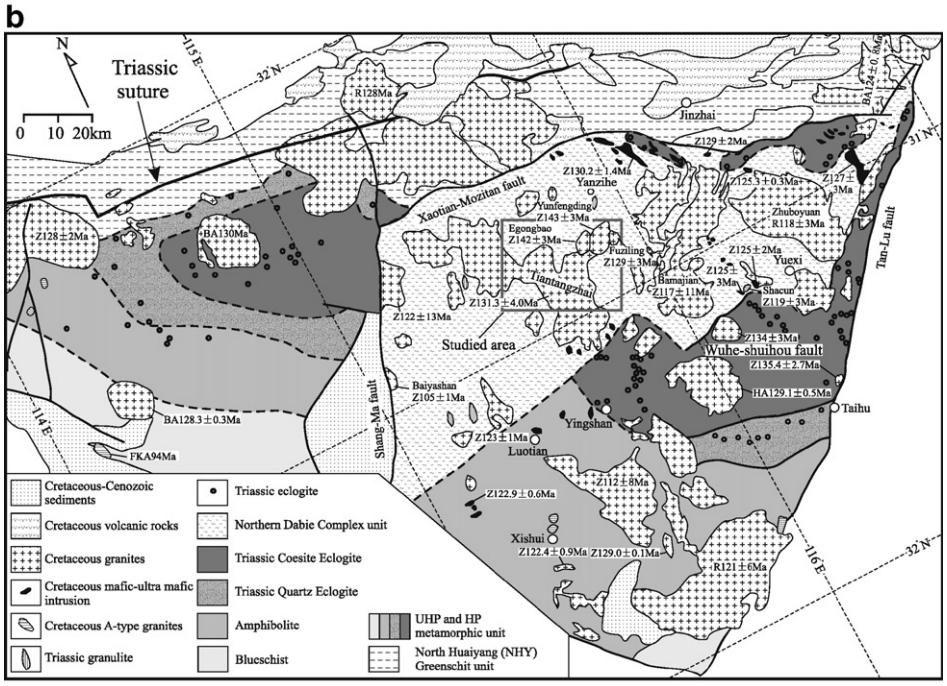
b
N
Triassic suture
0 10 20km
115°E
32°N
31°N
114°E
116°E
R128Ma
Jinzhai
Z129±2Ma
Z130.2±1.4Ma
Yanzihe
Yunfengding
Z143±3Ma
Egongbao
Z142±3Ma
Fuziling
Z129±3Ma
Xiaotian-Mozitan fault
Z128±2Ma
BA130Ma
Tiantangzhai
Z131.3±4.0Ma
Z122±13Ma
Studied area
Z125.3±0.3Ma
Z127±3Ma
Zhuboyuan
R118±3Ma
Z125±2Ma
Yuexi
Banajian
Z117±11Ma
Shacun
Z119±3Ma
Tan-Lu fault
Z134±3Ma
Wuhe-shuihou fault
Z135.4±2.7Ma
HA129.1±0.5Ma
Taihu
Baiyashan
Z105±1Ma
Shang-Ma fault
BA128.3±0.3Ma
FKA94Ma
Yingshan
Z123±1Ma
Luotian
Z112±8Ma
Z122.9±0.6Ma
Xishui
Z122.4±0.9Ma
Z129.0±0.1Ma
R121±6Ma
Cretaceous-Cenozoic sediments
Cretaceous volcanic rocks
Cretaceous granites
Cretaceous mafic-ultra mafic intrusion
Cretaceous A-type granites
Triassic granulite
Triassic eclogite
Northern Dabie Complex unit
Triassic Coesite Eclogite
Triassic Quartz Eclogite
Amphibolite
Blueschist
UHP and HP metamorphic unit
North Huaiyang (NHY) Greenschit unit

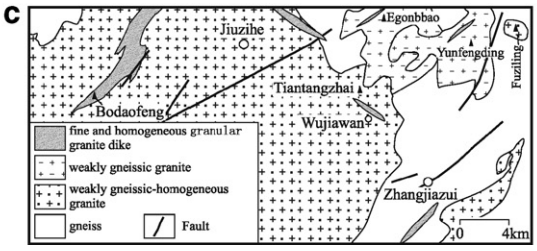
c
Jiuzihe
Egonbbao
Yunfengding
Fuziling
Tiantangzhai
Bodaofeng
Wujiawan
Zhangjiazui
fine and homogeneous granular granite dike
weakly gneissic granite
weakly gneissic-homogeneous granite
gneiss
Fault
0 4km

granitic and minor mafic–ultramafic intrusive rocks, the NDC unit also contains Neoproterozoic (700–800 Ma) tonalite–trondhjemite–granodiorite orthogneisses and amphibolites (Hacker et al., 1998, 2000; Zheng et al., 2003; Bryant et al., 2004), minor metasedimentary rocks (e.g., marble, quartzite, calc-silicates and biotite schist) and granulites, and rare peridotites (e.g., Zhang et al., 1996; Bryant et al., 2004). The peridotites occur as lenses along the northern borders of the NDC, and are considered to be deformed Alpine-type metaperidotites (e.g., Zhang et al., 1996). Recently, some eclogites and microdiamond-bearing eclogites have also been discovered in the northernmost NDC just south of the Xiaotian–Mozitan fault (Fig. 1b) (e.g., Xu et al., 2003; Hacker et al., 2004; Liu et al., 2005) where they overlie the gneisses (e.g., Suo et al., 2003). Geological observations indicate that these eclogites and microdiamond-bearing eclogites are always separated from the underlying gneiss by a detachment fault (Suo et al., 2003). Therefore, the peridotites and eclogites may represent erosional remnants of the portion of the UHP slab that penetrated most deeply into the mantle and then experienced exhumation along the northern (i.e., Xiaotian–Mozitan) fault (Suo et al., 2003; Bryant et al., 2004; Hacker et al., 2004).

The UHP–HP unit contains four sub-units from north to south: coesite eclogite, quartz eclogite, amphibolite and blueschist (Fig. 1b). Both coesite eclogite and quartz eclogite sub-units are mainly composed of eclogites, garnet-bearing peridotites, jadeite quartzites, marble, garnet-mica shcists and gneisses. The eclogites occur as lenses, boundins, enclaves or layers in ortho- and paragneisses gneisses of granitic compositions, marbles or garnet-mica schists, and ultramafic rocks (e.g., Jahn, 1998). The coesite eclogite unit is characterized by the occurrence of UHP metamorphic rocks such as coesite- and even microdiamond-bearing eclogites (e.g., Liou et al., 1996; Xu et al., 2003), whereas the quartz eclogite unit lacks such minerals (Hacker et al., 1998, 2000; Ratschbacher et al., 2000). The amphibolite unit contains amphibolite-facies hornblende-rich orthogneisses. The epidote-bearing blueschist unit occurs in the southernmost part of the UHP–HP unit. Geochronological studies indicate that the UHP–HP metamorphism took place between 245 and 210 Ma (Rowley et al., 1997; Hacker et al., 1998, 2000; Li et al., 2000; Ayers et al., 2002; Liu et al., 2004, 2006; Wan et al., 2005, and references therein) and was followed by "rapid cooling" from peak metamorphic temperatures to ~200 °C between 210 and 170 Ma (Hacker et al., 1998, 2000; Li et al., 2000; Liu et al., 2004).

The Hong'an area to the west of the Shang–Ma fault contains tectonic units similar to the Dabie area but lacks a middle unit similar to the NDC (Fig. 1b). Structural evidence and geochronological data suggest that the difference is due to the result of stronger Cretaceous (~140–120 Ma) NW–SE extension in the Dabie area (Hacker et al., 1998, 2000; Ratschbacher et al., 2000). Hacker et al. (1998) suggested that the extension in the NDC area doubled the width of crust in the Dabie area, resulting in the present 140-km wide mountain belt. Therefore, the NDC has consistently been interpreted as a Cretaceous asymmetric structural dome or metamorphic core complex (Hacker et al., 1998, 2004; Ratschbacher et al., 2000; Bryant et al., 2004).

All three units of the Dabie Orogen are also characterized by large-scale Cretaceous granitic and minor mafic–ultramafic intrusions (e.g., Ma et al., 1998; Zhang et al., 2002a; Fan et al., 2004). Previous zircon geochronology data (e.g., Xue et al., 1997; Hacker et al., 1998; Jahn et al., 1999; Bryant et al., 2004; Zhao et al., 2005) and this study suggest that these Cretaceous granitic and mafic–ultramafic intrusions have ages of 143–94 and 130–123 Ma, respectively (Fig. 1b). Two kinds of Cretaceous granitic rocks in the Jiuzihe–Zhangjiazui area of the NDC are distinguished on the basis of their textures and ages. Early granitoids emplaced between 143 and 129 Ma are (weakly) gneissic and include the Tiangtnagzhai, Yunfengding, Egongbao and Fuziling intrusions (Fig. 1b and c). The Tiantangzhai intrusion is the biggest of the early granites with an outcrop area of more than 400 $km^2$ whereas the smallest is the Fuziling intrusion, which has an outcrop area of about 1.8 $km^2$. Late granitoids were emplaced between 118 and 94 Ma and display relatively homogeneous textures. They include the Baiyashan, Zhuboyuan, and Baimajian intrusions (Xue et al., 1997; Hacker et al., 1998; Ma et al., 1998; Zhang et al., 2002a; Bryant et al., 2004; This study). Late dikes (e.g., in the Bodaofeng and Wujiawan areas: Fig. 1c) intrude all the four of the early granitoid intrusions (Fig. 1c), and exhibit homogeneous structures similar to the late granites (e.g., Bryant et al., 2004). The gneissic structure in the early granites probably reflects the fact that they were emplaced during the formation of the northern Dabie metamorphic core complex whereas the younger homogeneous granites and dikes post-dated formation of the core complex.

## 3. PETROGRAPHY

The early granites are all weakly gneissic but display some variation in K-feldspar phenocryst content and groundmass composition. The Egongbao granites exhibit inequigranular texture with coarse granular (~1 cm) phenocryst K-feldspar (1–5%, by volume) and medium-grained granular (0.35–0.1 cm) groundmass minerals (K-feldspar, plagioclase, quartz, biotite, and accessory sphene, magnetite and zircon). The Yunfengding granite exhibits a similar texture but with coarser (1.5–2 cm) and more abundant phenocryst K-feldspar (5–30%) in a medium- to fine-grained granular (0.3–0.05 cm) groundmass minerals (plagioclase, K-feldspar, quartz, biotite, minor hornblende, and accessory magnetite, sphene and zircon). The early Tiantangzhai intrusion is composed of weakly gneissic-homogeneous granite-granodiorites and minor trondhjemites. The granite-granodiorites exhibit inequigranular texture with coarse granular (0.6-2 cm) K-feldspar phenocrysts and granular fine- to medium-grained (0.35–0.05 cm) K-feldspar, plagioclase, quartz, biotite, hornblende, minor albite, and accessory sphene, magnetite and zircon. The K-feldspar phenocrysts are distributed unevenly in the intrusion and their abundance ranges from 1% to 30% by volume. The Fuziling intrusion is composed of weakly gneissic-homogeneous monzo-granites that display medium- to fine-grained

granular (0.25–0.05 cm) texture and consist of plagioclase, K-feldspar, quartz, biotite, and accessory magnetite and zircon.

The late granites (e.g., the Baiyashan, Baimajian and Zhuboyuan intrusions: Ma et al., 1998; Bryant et al., 2004) and granitic dikes exhibit homogeneous and fine granular (0.12–0.05 cm) texture and mainly consist of K-feldspar, quartz, plagioclase, biotite, and accessory minerals (magnetite, sphene, and zircon).

## 4. ANALYTICAL METHODS

Samples from the four early granites and associated late granite dikes were examined by optical microscopy and unaltered or the least-altered samples were selected for further analysis.

Zircons were separated using conventional heavy liquid and magnetic separation techniques. Representative zircon grains were handpicked and mounted in an epoxy resin disc, and then polished and coated with gold film. Their internal morphology was examined using cathodoluminescence prior to U–Pb isotopic analysis. The U–Pb isotopic analyses were performed using the sensitive high-resolution ion microprobe (SHRIMP-II) at the Chinese Academy of Geological Sciences, Beijing, following the procedures described in Jian et al. (2003) and Liu et al. (2006). For the zircon analyses, nine ion species of $Zr_2O^+$, $^{204}Pb^+$, background, $^{206}Pb^+$, $^{207}Pb^+$, $^{208}Pb^+$, $U^+$, $Th^+$, $ThO^+$, and $UO^+$ were measured on a single electron multiplier by cyclic stepping of the magnetic field, recording the mean ion counts of every five scans. A primary ion beam of c. 4.5 nA, 10 kV $O_2^-$ and c. 25–30 μm spot diameter was used. Interelement fractionation in the ion emission of zircon was corrected for using the RSES reference standard TEM (417 Ma). The software of Ludwig (SQUID1.0) and accompanying ISOPLOT were used for data processing (Ludwig, 2001). Ages were calculated using the constants recommended by IUGS (Steiger and Jager, 1977). Uncertainties in the ages listed in Table 1 are cited as $1\sigma$, and the weighted mean ages are quoted at the 95% confidence level.

Except for sample TS-10T, major elements were analyzed at the Hubei Institute of Geology and Mineral Resources by wavelength dispersive X-ray fluorescence spectrometry. Analytical errors are usually less than 1%. FeO contents of the samples were determined by conventional wet chemical titration methods. The analytical procedures used to determine FeO and the other major elements are described in detail by Gao et al. (1995). Major elements of sample TS-10T were determined using a Varian Vista PRO ICP-AES at the Guangzhou Institute of Geochemistry, Chinese Academy of Sciences. Details of the analytical procedures were described by Li et al. (2002). Trace elements of some samples (Table 2), including the rare earth elements (REE), were analyzed using a Perkin-Elmer ELAN 6000 inductively-coupled plasma source mass spectrometer (ICP-MS) at the Guangzhou Institute of Geochemistry, Chinese Academy of Sciences following procedures described by Li et al. (2002). Analytical precision for most elements is better than 3%. Trace elements of the other samples (Table 2) were analyzed at the Hubei Institute of Geology and Mineral Resources by ICP-AES as described in detail by Gao et al. (1995) and Ma et al. (1998, 2000). The analytical precision for REE and Y is better than 4% and 5–10% for other trace elements.

Sr and Nd isotopic compositions were determined using a Finnigan MAT-262 mass spectrometer operated in a static multi-collector mode at the Institute of Geology and Geophysics, Chinese Academy of Sciences, Beijing, following procedures similar to those of Zhang et al. (2002b). The $^{87}Sr/^{86}Sr$ ratio of NBS standard 987 and the $^{143}Nd/^{144}Nd$ ratio of the La Jolla standard measured during the period of analysis were $0.710234 \pm 7$ ($2\sigma_m$) and $^{143}Nd/^{144}Nd = 0.511838 \pm 8$ ($2\sigma_m$), respectively. Procedural blanks were about 50 pg for Sm and Nd and 0.2–0.5 ng for Rb and Sr. The Rb, Sr, Sm, and Nd concentrations were also measured by isotope dilution; the concentrations exhibit good agreement with the data obtained by ICP-MS. The measured $^{143}Nd/^{144}Nd$ and $^{86}Sr/^{88}Sr$ ratios are normalized to $^{146}Nd/^{144}Nd = 0.7219$ and $^{86}Sr/^{88}Sr = 0.1194$, respectively.

## 5. RESULTS

### 5.1. SHRIMP U–Pb zircon geochronology

Zircons were analyzed from samples of three of the early granites (the Egongbao, Yunfengding, and Fuziling intrusions: EGB-8, YFD-8, and FZL-3). The zircons are mostly prismatic (about 150–350 μm length) with well-developed pyramidal faces. Cathodoluminescence images clearly display oscillatory zoning most crystals and the presence of old cores in some zircons. The results of SHRIMP U–Pb zircon analyses are listed in Table 1 and illustrated on a concordia plot in Fig. 2.

Twelve analyses of zircons from the Egongbao sample EGB-8 yield $^{206}Pb/^{238}U$ a single age population of 132–145 Ma, with a weighted mean age of $142 \pm 3$ Ma ($2\sigma$) (Table 1, and Fig. 2a and b), which is the best estimate for crystallization ages of the Egongbao granites. In addition, two zircons from sample EGB-8 also gave two discordant ($1566 \pm 41$ and $160 \pm 5$ Ma) ages (Fig. 2a). Ten analyses of zircons from Yunfengding sample YFD-8 yield $^{206}Pb/^{238}U$ a single age population of 132–149 Ma, with a weighted mean age of $143 \pm 3$ Ma ($2\sigma$) (Table 1 and Fig. 2c), which is the best estimate for crystallization ages of the Yunfengding granites. Core and rim analyses of one zircon from sample YFD-8 also gave a concordant inherited age ($1710 \pm 39$ Ma) and a concordant magmatic crystallization age ($132 \pm 5$ Ma), respectively (Fig. 2c). Additionally, thin rims on four zircon grains with 142–149 Ma cores yield $^{206}Pb/^{238}U$ a single age population of 113–119 Ma, with a weighted mean age of $116 \pm 4$ Ma ($2\sigma$) (Table 1 and Fig. 2c). The rim age ($116 \pm 4$ Ma) is similar to the crystallization ages (117–118 Ma) of the late Baimajian and Zhuboyuan granites in the NDC (Fig. 1b; Zhang et al., 2002a; Bryant et al., 2004), indicating that late magmatism might have caused recrystallization of the rims of some zircons in the Yunfengding granites. Fourteen analyses of zircons from the Fuziling sample FZL-3 yield

Table 1
SHRIMP U–Pb isotopic data for zircons from the Egongbao, Yunfengding, and Fuziling adakitic granites

| Spot | $^{206}$Pbc (%) | U ppm | Th ppm | $^{232}$Th /$^{238}$U | $^{206}$Pb* (ppm) | $^{206}$Pb/$^{238}$U (age, Ma) | $^{207}$Pb* /$^{206}$Pb* | ±% | $^{207}$Pb* /$^{235}$U | ±% | $^{206}$Pb* /$^{238}$U | ±% |
|---|---|---|---|---|---|---|---|---|---|---|---|---|
| *EGB-8 (Egongbao)* | | | | | | | | | | | | |
| C1.1 | — | 2118 | 338 | 0.17 | 37.9 | 132.1 ± 3.4 | 0.0491 | 4.0 | 0.1401 | 4.7 | 0.02071 | 2.6 |
| C2.1 | — | 482 | 113 | 0.24 | 8.84 | 132.9 ± 3.7 | 0.0508 | 11 | 0.146 | 12 | 0.02084 | 2.8 |
| C3.1 | — | 3162 | 567 | 0.19 | 65.2 | 152.0 ± 3.8 | 0.0481 | 2.9 | 0.1583 | 3.9 | 0.02386 | 2.5 |
| C4.1 | — | 800 | 385 | 0.50 | 14.9 | 136.5 ± 3.6 | 0.0506 | 7.9 | 0.149 | 8.4 | 0.02140 | 2.6 |
| C5.1 | — | 1544 | 124 | 0.08 | 27.4 | 130.4 ± 3.3 | 0.0504 | 4.3 | 0.1419 | 5.0 | 0.02044 | 2.5 |
| C6.1 | — | 347 | 68 | 0.20 | 7.07 | 145.2 ± 4.4 | 0.051 | 22 | 0.161 | 22 | 0.02277 | 3.0 |
| C7.1 | — | 1736 | 353 | 0.21 | 33.9 | 144.6 ± 3.6 | 0.0531 | 3.0 | 0.1663 | 3.9 | 0.02269 | 2.5 |
| C8.1 | — | 417 | 228 | 0.57 | 8.08 | 142.8 ± 3.9 | 0.0765 | 8.3 | 0.236 | 8.8 | 0.02241 | 2.8 |
| C9.1 | — | 311 | 81 | 0.27 | 6.18 | 141.4 ± 4.3 | 0.063 | 18 | 0.192 | 18 | 0.02217 | 3.0 |
| C10.1 | — | 295 | 128 | 0.45 | 5.77 | 139.1 ± 4.2 | 0.057 | 19 | 0.170 | 19 | 0.02180 | 3.0 |
| C11.1 | — | 362 | 139 | 0.40 | 7.31 | 144.7 ± 4.5 | 0.061 | 21 | 0.190 | 21 | 0.02271 | 3.1 |
| C12.1 | — | 323 | 91 | 0.29 | 6.39 | 142.1 ± 5.5 | 0.0585 | 15 | 0.180 | 15 | 0.02229 | 3.9 |
| C13.1 | — | 671 | 46 | 0.07 | 159 | 1,566 ± 41 | 0.1167 | 1.1 | 4.42 | 3.2 | 0.2749 | 3.0 |
| C14.1 | — | 301 | 69 | 0.24 | 6.43 | 159.7 ± 4.6 | 0.1076 | 3.5 | 0.372 | 4.6 | 0.02508 | 2.9 |
| C15.1 | — | 666 | 213 | 0.33 | 13.0 | 141.7 ± 3.8 | 0.0509 | 9.1 | 0.156 | 9.5 | 0.02222 | 2.7 |
| C16.1 | 0.63 | 2169 | 234 | 0.11 | 41.2 | 140.4 ± 3.5 | 0.0532 | 3.1 | 0.1614 | 4.0 | 0.02202 | 2.5 |
| *YFD-8 (Yunfengding)* | | | | | | | | | | | | |
| L1.1 | 7.92 | 145 | 2 | 0.01 | 3.09 | 145.8 ± 6.1 | 0.0531 | 16 | 0.168 | 17 | 0.02288 | 3.3 |
| L1.2 | 0.42 | 975 | 593 | 0.63 | 15.7 | 119.4 ± 3.9 | 0.0541 | 4.3 | 0.1393 | 5.1 | 0.01869 | 2.8 |
| L2.1 | 0.41 | 905 | 95 | 0.11 | 18.2 | 148.5 ± 3.9 | 0.0486 | 2.6 | 0.1562 | 3.7 | 0.02331 | 2.6 |
| L2.2 | 1.74 | 301 | 33 | 0.11 | 4.67 | 113.3 ± 3.4 | 0.0474 | 6.1 | 0.1159 | 6.7 | 0.01772 | 2.9 |
| L3.1 | 1.45 | 301 | 7 | 0.02 | 5.83 | 141.8 ± 4.1 | 0.0483 | 5.6 | 0.1481 | 6.3 | 0.02224 | 2.8 |
| L3.2 | 0.59 | 931 | 100 | 0.11 | 14.4 | 114.1 ± 3.2 | 0.0487 | 4.6 | 0.1200 | 5.4 | 0.01786 | 2.8 |
| L4.1 | 0.58 | 1064 | 160 | 0.16 | 21.0 | 145.4 ± 3.8 | 0.0467 | 3.6 | 0.1470 | 4.4 | 0.02281 | 2.6 |
| L5.1 | 1.35 | 484 | 49 | 0.10 | 9.01 | 136.4 ± 3.6 | 0.0507 | 4.6 | 0.1495 | 5.3 | 0.02139 | 2.6 |
| L6.1 | 1.32 | 512 | 157 | 0.32 | 10.2 | 145.9 ± 4.0 | 0.0467 | 3.1 | 0.1475 | 4.0 | 0.02290 | 2.6 |
| L7.1 | 0.77 | 1082 | 112 | 0.11 | 17.3 | 118.3 ± 3.3 | 0.0460 | 5.2 | 0.1174 | 5.9 | 0.01852 | 2.7 |
| L7.2 | 2.97 | 123 | 6 | 0.05 | 2.43 | 142.0 ± 4.8 | 0.0472 | 10 | 0.145 | 11 | 0.02227 | 3.2 |
| L8.1 | — | 1701 | 313 | 0.19 | 443 | 1,710 ± 39 | 0.2055 | 0.65 | 8.61 | 2.6 | 0.3039 | 2.5 |
| L8.2 | 4.71 | 199 | 11 | 0.06 | 3.71 | 131.8 ± 4.6 | 0.045 | 23 | 0.127 | 23 | 0.02065 | 3.1 |
| L9.1 | 0.62 | 630 | 47 | 0.08 | 12.2 | 142.8 ± 4.0 | 0.0503 | 4.4 | 0.1554 | 5.2 | 0.02240 | 2.8 |
| L10.1 | 0.53 | 1266 | 156 | 0.13 | 25.0 | 145.9 ± 3.7 | 0.04737 | 2.0 | 0.1495 | 3.2 | 0.02289 | 2.5 |
| *Fuzl-3 (Fuziling)* | | | | | | | | | | | | |
| M1.1 | 10.30 | 96 | 118 | 1.27 | 1.91 | 132.9 ± 7.3 | 0.041 | 39 | 0.119 | 39 | 0.02083 | 3.5 |
| M2.1 | 12.13 | 128 | 137 | 1.11 | 2.46 | 125.7 ± 5.9 | 0.031 | 47 | 0.083 | 47 | 0.01969 | 3.0 |
| M3.1 | 2.40 | 281 | 193 | 0.71 | 5.73 | 147.8 ± 4.9 | 0.0474 | 4.7 | 0.1515 | 5.5 | 0.02320 | 2.9 |
| M4.1 | 7.33 | 153 | 89 | 0.60 | 2.77 | 124.6 ± 4.7 | 0.0472 | 14 | 0.127 | 15 | 0.01951 | 3.0 |
| M5.1 | 4.96 | 333 | 806 | 2.50 | 5.83 | 123.5 ± 6.3 | 0.0306 | 7.8 | 0.0816 | 8.3 | 0.01934 | 2.7 |
| M6.1 | 2.61 | 427 | 230 | 0.56 | 8.54 | 144.6 ± 4.9 | 0.0471 | 4.2 | 0.1473 | 5.2 | 0.02268 | 3.0 |
| M7.1 | 4.05 | 324 | 567 | 1.81 | 5.62 | 123.6 ± 5.3 | 0.0382 | 13 | 0.102 | 13 | 0.01936 | 2.8 |
| M8.1 | 7.74 | 94 | 42 | 0.46 | 1.80 | 130.7 ± 5.5 | 0.048 | 38 | 0.136 | 38 | 0.02048 | 3.3 |
| M9.1 | 0.69 | 1719 | 348 | 0.21 | 28.9 | 124.3 ± 3.2 | 0.04761 | 1.8 | 0.1278 | 3.1 | 0.01946 | 2.5 |
| M10.1 | 1.89 | 289 | 131 | 0.47 | 5.04 | 127.1 ± 4.0 | 0.0509 | 9.3 | 0.140 | 9.7 | 0.01992 | 2.8 |
| M11.1 | 0.62 | 1242 | 119 | 0.10 | 22.3 | 132.8 ± 3.6 | 0.0489 | 3.3 | 0.1403 | 4.2 | 0.02082 | 2.6 |
| M12.1 | 0.45 | 1947 | 76 | 0.04 | 36.1 | 137.2 ± 3.6 | 0.04969 | 1.7 | 0.1474 | 3.1 | 0.02151 | 2.6 |
| M13.1 | 0.41 | 2157 | 329 | 0.16 | 39.2 | 134.4 ± 3.4 | 0.04728 | 1.6 | 0.1374 | 3.0 | 0.02107 | 2.5 |
| M14.1 | 11.71 | 128 | 46 | 0.37 | 2.38 | 121.4 ± 5.8 | 0.040 | 44 | 0.104 | 44 | 0.01902 | 3.1 |
| M15.1 | 5.03 | 244 | 334 | 1.42 | 4.44 | 128.3 ± 5.5 | 0.0435 | 15 | 0.120 | 15 | 0.02010 | 3.0 |
| M16.1 | 4.29 | 214 | 96 | 0.46 | 3.96 | 131.1 ± 4.4 | 0.0501 | 12 | 0.142 | 12 | 0.02054 | 2.8 |

(1) Errors are 1-sigma; $Pb_c$ and $Pb^*$ indicate the common and radiogenic portions, respectively; (2) error in standard calibration was 0.33% (not included in above errors but required when comparing data from different mounts); (3) common Pb corrected using measured $^{204}$Pb for the Egongbao intrusion; (4) common Pb corrected by assuming $^{206}$Pb/$^{238}$U–$^{208}$Pb/$^{232}$Th age-concordance for the Yunfengding and Fuziling intrusions.

$^{206}$Pb/$^{238}$U a single age population of 122–137 Ma, with a weighted mean age of 129 ± 3 Ma (2$\sigma$) (Table 1 and Fig. 2d), which is the best estimate for crystallization ages of the Fuziling granites. Two zircons from sample FZL-3 also give inherited ages (148 ± 5 and 145 ± 5 Ma: Fig. 2d).

Table 2
Major (wt%) and trace (ppm) elements concentrations for the adakitic granites and late dikes in the Northern Dabie Complex

| Intrusion sample | Yunfengding | | | | | | | | | |
|---|---|---|---|---|---|---|---|---|---|---|
| | YFD-1[a] | YFD-2[a] | YFD-3[a] | YFD-5[a] | YFD-8[a] | YFD-9[a] | Y-1[a] | 906-1c | 231-1b | 237-1c |
| $SiO_2$ | 68.22 | 67.57 | 68.60 | 67.31 | 67.90 | 67.44 | 67.50 | 67.19 | 70.17 | 68.91 |
| $TiO_2$ | 0.50 | 0.60 | 0.45 | 0.55 | 0.57 | 0.54 | 0.51 | 0.56 | 0.34 | 0.44 |
| $Al_2O_3$ | 15.75 | 15.58 | 15.83 | 15.87 | 15.61 | 16.00 | 15.62 | 15.79 | 15.16 | 15.42 |
| $Fe_2O_3$ | 0.79 | 1.10 | 0.80 | 0.94 | 1.01 | 0.94 | 1.03 | 1.38 | 0.86 | 1.00 |
| FeO | 1.78 | 1.85 | 1.48 | 1.83 | 1.92 | 1.85 | 1.78 | 1.41 | 0.86 | 1.24 |
| MnO | 0.04 | 0.04 | 0.04 | 0.04 | 0.04 | 0.04 | 0.03 | 0.03 | 0.02 | 0.02 |
| MgO | 1.03 | 1.13 | 0.87 | 1.19 | 1.23 | 1.13 | 1.07 | 1.14 | 0.75 | 1.06 |
| CaO | 2.31 | 2.54 | 2.14 | 2.49 | 2.39 | 2.31 | 2.27 | 2.68 | 1.75 | 1.75 |
| $Na_2O$ | 4.47 | 4.25 | 4.27 | 4.28 | 4.38 | 4.20 | 4.63 | 4.56 | 4.39 | 4.43 |
| $K_2O$ | 3.77 | 3.65 | 4.06 | 4.06 | 3.58 | 4.17 | 4.09 | 3.60 | 4.24 | 4.41 |
| $P_2O_5$ | 0.16 | 0.16 | 0.10 | 0.13 | 0.17 | 0.14 | 0.18 | 0.23 | 0.12 | 0.16 |
| $H_2O$ | 0.68 | 1.02 | 0.76 | 0.73 | 0.71 | 0.70 | 0.77 | 1.05 | 0.41 | 0.31 |
| $CO_2$ | 0.07 | 0.07 | 0.07 | 0.07 | 0.07 | 0.05 | 0.09 | 0.07 | 0.08 | 0.07 |
| Σ | 99.57 | 99.56 | 99.47 | 99.49 | 99.58 | 99.51 | 99.57 | 99.69 | 99.15 | 99.22 |
| Cr | 11.9 | 11.8 | 15.2 | 23.8 | 12.3 | 16.7 | 4.99 | 19.0 | 19.3 | 19.3 |
| Ni | 7.94 | 7.74 | 7.62 | 9.56 | 9.10 | 8.31 | 6.70 | 8.30 | 5.90 | 9.50 |
| Co | 5.43 | 7.61 | 6.39 | 6.09 | 6.51 | 5.85 | 6.39 | 8.50 | 5.20 | 7.10 |
| Sc | 3.18 | 3.79 | 3.11 | 3.96 | 3.63 | 2.73 | 3.35 | 0.00 | 0.00 | 0.00 |
| V | 39.4 | 54.5 | 44.9 | 45.6 | 49.2 | 41.1 | 42.9 | 54.7 | 27.2 | 35.9 |
| Pb | 24.5 | 23.1 | 29.2 | 22.9 | 21.6 | 23.6 | 21.4 | 27.6 | 23.3 | 24.9 |
| Rb | 79.3 | 77.4 | 106 | 82.5 | 79.7 | 88.2 | 80.3 | 78.0 | 82.6 | 91.6 |
| Cs | 0.424 | 0.379 | 0.498 | 0.817 | 0.618 | 0.603 | 0.344 | | | |
| Ba | 2047 | 2155 | 3027 | 2175 | 2022 | 2476 | 2287 | 2115 | 1890 | 2260 |
| Sr | 983 | 981 | 1301 | 941 | 1000 | 950 | 1052 | 956 | 817 | 928 |
| Ga | 20.6 | 20.7 | 25.4 | 19.6 | 20.5 | 19.7 | 22.3 | | | |
| Ta | 0.361 | 0.439 | 0.282 | 0.369 | 0.344 | 0.306 | 0.379 | | 0.27 | 0.71 |
| Nb | 6.56 | 7.94 | 6.51 | 7.13 | 6.84 | 5.93 | 6.75 | 6.8 | 4.6 | 7.3 |
| Hf | 2.55 | 2.43 | 5.64 | 2.08 | 2.38 | 1.92 | 2.79 | | 3.9 | 6.8 |
| Zr | 96.8 | 91.3 | 219 | 80.0 | 89.3 | 73.1 | 93.0 | 203 | 137 | 196 |
| Y | 6.19 | 7.90 | 6.16 | 7.69 | 7.21 | 5.57 | 6.33 | 6.27 | 3.87 | 4.89 |
| Th | 11.2 | 13.3 | 17.8 | 11.9 | 13.4 | 12.5 | 13.3 | 12.7 | 8.60 | 11.2 |
| U | 0.316 | 0.320 | 0.352 | 0.298 | 0.358 | 0.298 | 0.375 | | 0.39 | 0.62 |
| La | 44.0 | 55.1 | 65.6 | 44.9 | 51.9 | 48.5 | 52.9 | 55.7 | 35.3 | 62.6 |
| Ce | 78.9 | 98.9 | 115 | 80.8 | 95.3 | 83.8 | 96.1 | 103 | 64.8 | 113 |
| Pr | 9.04 | 11.3 | 12.9 | 9.23 | 10.8 | 9.19 | 10.1 | 11.0 | 7.29 | 12.3 |
| Nd | 31.6 | 40.0 | 44.0 | 32.2 | 37.5 | 30.8 | 35.8 | 38.5 | 24.1 | 39.3 |
| Sm | 4.59 | 5.91 | 5.99 | 4.72 | 5.35 | 3.94 | 5.73 | 5.60 | 3.56 | 5.67 |
| Eu | 1.21 | 1.34 | 1.63 | 1.14 | 1.26 | 1.09 | 1.61 | 1.31 | 0.910 | 1.26 |
| Gd | 2.45 | 3.02 | 2.77 | 2.57 | 2.85 | 1.96 | 3.63 | 3.30 | 2.15 | 3.07 |
| Tb | 0.320 | 0.417 | 0.353 | 0.350 | 0.363 | 0.266 | 0.393 | 0.41 | 0.26 | 0.36 |
| Dy | 1.32 | 1.71 | 1.42 | 1.54 | 1.54 | 1.14 | 1.54 | 1.51 | 0.930 | 1.18 |
| Ho | 0.203 | 0.259 | 0.207 | 0.254 | 0.237 | 0.183 | 0.242 | 0.257 | 0.170 | 0.205 |
| Er | 0.52 | 0.64 | 0.50 | 0.665 | 0.60 | 0.46 | 0.59 | 0.52 | 0.41 | 0.43 |
| Tm | 0.068 | 0.080 | 0.062 | 0.086 | 0.077 | 0.058 | 0.074 | 0.07 | 0.05 | 0.06 |
| Yb | 0.400 | 0.474 | 0.379 | 0.521 | 0.478 | 0.358 | 0.456 | 0.35 | 0.30 | 0.34 |
| Lu | 0.063 | 0.072 | 0.060 | 0.074 | 0.071 | 0.055 | 0.058 | 0.05 | 0.04 | 0.06 |
| | Egongbao | | | | | | | | Tiantangzhai | |
| | 158-1c | 1794-1b | EGB-1[a] | EGB-2[a] | EGB-3[a] | EGB-4[a] | EGB-7[a] | EGB-8[a] | 1071 | 1095 | Pan2 |
| $SiO_2$ | 68.95 | 72.20 | 70.48 | 69.02 | 76.24 | 71.90 | 71.66 | 72.94 | 70.53 | 70.53 | 71.44 |
| $TiO_2$ | 0.36 | 0.26 | 0.40 | 0.53 | 0.23 | 0.29 | 0.24 | 0.21 | 0.27 | 0.31 | 0.26 |
| $Al_2O_3$ | 15.73 | 14.17 | 14.20 | 15.27 | 12.16 | 14.33 | 14.77 | 14.02 | 15.52 | 14.96 | 14.46 |
| $Fe_2O_3$ | 1.00 | 0.84 | 1.57 | 1.00 | 0.48 | 0.48 | 0.85 | 0.54 | 0.87 | 1.02 | 0.89 |
| FeO | 1.06 | 0.73 | 1.85 | 1.45 | 0.77 | 1.22 | 0.88 | 1.03 | 0.61 | 0.91 | 0.85 |
| MnO | 0.02 | 0.03 | 0.06 | 0.05 | 0.01 | 0.02 | 0.04 | 0.02 | 0.02 | 0.03 | 0.02 |
| MgO | 0.65 | 0.49 | 1.06 | 0.63 | 0.25 | 0.53 | 0.46 | 0.44 | 0.35 | 0.65 | 0.63 |
| CaO | 1.85 | 1.86 | 2.59 | 1.84 | 0.73 | 1.28 | 1.50 | 1.52 | 1.89 | 1.96 | 1.84 |
| $Na_2O$ | 4.50 | 3.93 | 4.40 | 3.90 | 3.10 | 4.05 | 4.54 | 4.06 | 4.44 | 3.7 | 3.78 |
| $K_2O$ | 4.28 | 3.70 | 1.94 | 4.87 | 5.03 | 4.77 | 4.13 | 4.34 | 4.44 | 4.68 | 4.16 |
| $P_2O_5$ | 0.10 | 0.08 | 0.07 | 0.12 | 0.02 | 0.06 | 0.06 | 0.05 | 0.08 | 0.09 | 0.11 |

(*continued on next page*)

Table 2 (*continued*)

| | Egongbao | | | | | | | | Tiantangzhai | | |
|---|---|---|---|---|---|---|---|---|---|---|---|
| | 158-1c | 1794-1b | EGB-1[a] | EGB-2[a] | EGB-3[a] | EGB-4[a] | EGB-7[a] | EGB-8[a] | 1071 | 1095 | Pan2 |
| $H_2O$ | 0.67 | 1.42 | 1.05 | 0.83 | 0.44 | 0.60 | 0.49 | 0.46 | 0.42 | 0.62 | 0.42 |
| $CO_2$ | 0.04 | 0.07 | 0.07 | 0.05 | 0.07 | 0.09 | 0.09 | 0.14 | 0.02 | 0.01 | 0.01 |
| Σ | 99.21 | 99.78 | 99.74 | 99.56 | 99.53 | 99.62 | 99.71 | 99.77 | 99.46 | 99.47 | 98.87 |
| Cr | 16.8 | 10.1 | 20.6 | 11.5 | 2.86 | 6.04 | 5.76 | 5.70 | 7.0 | 6.0 | 18.6 |
| Ni | 5.40 | 3.00 | 6.61 | 4.65 | 1.46 | 2.57 | 3.46 | 2.73 | 4.6 | 5.2 | 6.6 |
| Co | 5.70 | 4.20 | 5.78 | 4.55 | 1.72 | 2.37 | 2.16 | 1.88 | 4.4 | 6.8 | 5.5 |
| Sc | 0.00 | 0.00 | 4.25 | 1.11 | 0.67 | 1.73 | 1.12 | 1.14 | | | |
| V | 26.6 | 25.4 | 53.3 | 40.0 | 8.87 | 14.7 | 13.8 | 12.3 | 27.0 | 37.9 | 25.6 |
| Pb | 21.2 | 31.6 | 18.8 | 33.0 | 23.3 | 23.6 | 55.3 | 33.4 | 26.3 | 31.3 | 30.9 |
| Rb | 95.7 | 93.0 | 55.8 | 126 | 86.1 | 91.1 | 154 | 90.8 | 116 | 134 | 98.3 |
| Cs | | | 0.476 | 0.526 | 0.301 | 0.443 | 0.481 | 0.450 | | | |
| Ba | 2070 | 1287 | 777 | 2349 | 2542 | 1928 | 1118 | 888 | 1925 | 2705 | 2368 |
| Sr | 761 | 485 | 621 | 704 | 503 | 477 | 502 | 393 | 677 | 662 | 749 |
| Ga | | | 19.2 | 20.2 | 13.4 | 18.1 | 23.8 | 18.9 | 21.2 | 13.7 | |
| Ta | 0.32 | | 0.288 | 0.678 | 0.132 | 0.186 | 1.17 | 0.472 | 1.0 | 1.7 | |
| Nb | 6.9 | 9.4 | 5.90 | 9.75 | 3.06 | 5.13 | 14.1 | 7.54 | 9.2 | 9.7 | 7.0 |
| Hf | 5.6 | | 3.34 | 3.25 | 3.26 | 3.43 | 4.73 | 2.86 | 4.2 | 5.5 | |
| Zr | 159 | 104 | 113 | 121 | 107 | 124 | 145 | 90.1 | 141 | 216 | 120 |
| Y | 3.94 | 5.31 | 8.40 | 6.95 | 2.83 | 4.71 | 6.18 | 4.93 | 8.00 | 8.64 | 6.63 |
| Th | 9.60 | 7.80 | 8.23 | 20.0 | 11.5 | 13.1 | 10.6 | 6.44 | 9.1 | 12.6 | 9.7 |
| U | 0.50 | | 0.427 | 0.661 | 0.294 | 0.443 | 1.96 | 0.657 | 1.7 | 1.9 | |
| La | 45.3 | 24.7 | 25.2 | 62.8 | 47.1 | 41.5 | 28.6 | 18.0 | 38.7 | 73.1 | 37.4 |
| Ce | 79.4 | 44.3 | 46.5 | 112 | 77.0 | 70.6 | 48.0 | 32.7 | 69.0 | 111.2 | 66.8 |
| Pr | 8.56 | 4.97 | 5.38 | 12.0 | 7.94 | 7.58 | 5.30 | 3.79 | 7.74 | 11.3 | 6.96 |
| Nd | 25.8 | 17.2 | 19.1 | 39.0 | 25.1 | 24.8 | 17.6 | 13.4 | 25.7 | 33.4 | 23.0 |
| Sm | 3.60 | 2.88 | 2.85 | 4.56 | 2.97 | 3.39 | 2.57 | 2.29 | 3.84 | 5.06 | 3.05 |
| Eu | 1.07 | 0.710 | 0.918 | 1.13 | 0.693 | 0.693 | 0.559 | 0.587 | 1.13 | 0.93 | 0.76 |
| Gd | 1.97 | 1.97 | 1.80 | 2.08 | 1.19 | 1.68 | 1.45 | 1.52 | 2.56 | 3.67 | 1.83 |
| Tb | 0.24 | 0.25 | 0.275 | 0.291 | 0.163 | 0.227 | 0.222 | 0.214 | 0.33 | 0.42 | 0.19 |
| Dy | 0.90 | 1.17 | 1.42 | 1.28 | 0.631 | 0.972 | 1.01 | 0.952 | 1.62 | 1.83 | 1.11 |
| Ho | 0.170 | 0.204 | 0.271 | 0.223 | 0.101 | 0.156 | 0.169 | 0.150 | 0.3 | 0.33 | 0.24 |
| Er | 0.36 | 0.43 | 0.762 | 0.60 | 0.27 | 0.39 | 0.469 | 0.366 | 0.81 | 0.85 | 0.65 |
| Tm | 0.05 | 0.06 | 0.117 | 0.084 | 0.039 | 0.051 | 0.067 | 0.048 | 0.12 | 0.14 | 0.10 |
| Yb | 0.26 | 0.33 | 0.780 | 0.555 | 0.297 | 0.334 | 0.490 | 0.295 | 0.73 | 0.73 | 0.73 |
| Lu | 0.05 | 0.05 | 0.128 | 0.093 | 0.056 | 0.053 | 0.078 | 0.044 | 0.11 | 0.10 | 0.13 |

| | Tiantangzhai | | | | | | | | | |
|---|---|---|---|---|---|---|---|---|---|---|
| | 1020 | TT17 | 1648 | H14 | 1016-1 | 1008-3 | Ts-28c | TT-21c-1 | 1019-2c | 1555-1c |
| $SiO_2$ | 74 | 72.37 | 72.03 | 73.38 | 70.30 | 65.78 | 66.30 | 70.98 | 69.29 | 71.15 |
| $TiO_2$ | 0.16 | 0.27 | 0.21 | 0.24 | 0.40 | 0.57 | 0.55 | 0.38 | 0.42 | 0.41 |
| $Al_2O_3$ | 13.73 | 13.66 | 14.62 | 13.61 | 15.00 | 17.13 | 17.34 | 14.58 | 16.08 | 14.73 |
| $Fe_2O_3$ | 0.87 | 0.97 | 0.67 | 0.67 | 1.42 | 1.82 | 1.57 | 1.49 | 1.16 | 1.32 |
| FeO | 0.79 | 0.93 | 0.75 | 0.55 | 1.10 | 1.44 | 1.45 | 1.16 | 1.24 | 1.28 |
| MnO | 0.05 | 0.05 | 0.03 | 0.01 | 0.04 | 0.06 | 0.06 | 0.03 | 0.03 | 0.04 |
| MgO | 0.55 | 0.75 | 0.22 | 0.59 | 0.66 | 0.91 | 0.71 | 0.79 | 0.37 | 0.55 |
| CaO | 2.02 | 2.36 | 1.72 | 1.36 | 1.91 | 2.61 | 2.48 | 2.13 | 2.07 | 1.97 |
| $Na_2O$ | 3.9 | 3.9 | 4.03 | 3.65 | 4.24 | 4.71 | 4.71 | 4.04 | 4.42 | 4.12 |
| $K_2O$ | 3.23 | 2.8 | 4.27 | 4.91 | 4.70 | 4.74 | 4.61 | 4.21 | 4.71 | 4.28 |
| $P_2O_5$ | 0.09 | 0.09 | 0.14 | 0.05 | 0.23 | 0.24 | 0.21 | 0.20 | 0.21 | 0.16 |
| $H_2O$ | 0.46 | 1.25 | 0.58 | 0.57 | 0.62 | 0.52 | 0.52 | 1.40 | 0.39 | 0.39 |
| $CO_2$ | 0.02 | 0.07 | 0.02 | | 0.01 | 0.02 | 0.05 | 0.09 | 0.08 | 0.04 |
| Σ | 99.87 | 99.47 | 99.29 | 99.59 | 100.63 | 100.54 | 100.57 | 101.49 | 100.47 | 100.43 |
| Cr | 2.5 | 5.1 | 13.7 | 10.8 | 8.6 | 14.6 | 6.2 | 9.0 | 20.0 | 19.2 |
| Ni | 3.0 | 1.1 | 1.3 | 2.5 | 4.4 | 5.6 | 3.1 | 3.1 | 7.1 | 6.0 |
| Co | 4.1 | 4.2 | 2.4 | 2.7 | 6.3 | 9.1 | 7.1 | 5.1 | 7.1 | 5.8 |
| Sc | | | | | | | | | 4.0 | 2.4 |
| V | 26.3 | 30.6 | 22.1 | 21.7 | 37.4 | 57.7 | 44.8 | 31.6 | 37.5 | 33.9 |
| Pb | 43.0 | 25.4 | 27.2 | 24.7 | 25.6 | 30.4 | 30.5 | 21.4 | 25.3 | 23.9 |
| Rb | 96.0 | | 33.1 | 93 | 102 | 129 | 98 | 105 | 91 | 86 |
| Cs | | | | | | | | | 2.7 | 1.9 |

Table 2 (*continued*)

| | Tiantangzhai | | | | | | | | | |
|---|---|---|---|---|---|---|---|---|---|---|
| | 1020 | TT17 | 1648 | H14 | 1016-1 | 1008-3 | Ts-28c | TT-21c-1 | 1019-2c | 1555-1c |
| Ba | 899 | 932 | 2210 | 2206 | 1629 | 2649 | 2285 | 1518 | 2442 | 1927 |
| Sr | 261 | 368 | 743 | 531 | 591 | 884 | 955 | 626 | 764 | 723 |
| Ga | 16.0 | | | | 21.0 | 26.2 | | | 18.6 | 18.1 |
| Ta | 0.90 | | | | 0.61 | 0.81 | | | 1.07 | 0.49 |
| Nb | 4.7 | 5.5 | 6.5 | 5.3 | 7.4 | 12.1 | 10.8 | 10.5 | 9.0 | 7.5 |
| Hf | 4.0 | | | | 7.3 | 8.4 | | | 6.7 | 6.9 |
| Zr | 104 | 121 | 155 | 92.0 | 238 | 262 | 230 | 205 | 180 | 189 |
| Y | 4.49 | 4.88 | 6.23 | 7.97 | 7.87 | 12.14 | 10.17 | 8.57 | 12.64 | 8.82 |
| Th | 6.5 | 6.9 | 10.1 | 6.4 | 10.1 | 12.3 | 14.5 | 11.4 | 11.1 | 7.40 |
| U | 0.7 | | | | 0.30 | 1.11 | | | 0.86 | 0.25 |
| La | 18.2 | 24.0 | 35.5 | 24.6 | 70.6 | 82.3 | 75.0 | 51.8 | 67.5 | 62.4 |
| Ce | 31.0 | 41.9 | 64.5 | 44.7 | 115 | 142 | 135 | 88.9 | 120 | 114 |
| Pr | 3.50 | 4.45 | 6.30 | 5.22 | 13.2 | 15.9 | 14.4 | 9.09 | 12.7 | 11.8 |
| Nd | 11.2 | 13.9 | 21.3 | 16.8 | 43.3 | 52.1 | 46.4 | 30.5 | 41.2 | 37.8 |
| Sm | 1.78 | 1.92 | 2.90 | 2.95 | 6.41 | 7.69 | 6.49 | 4.54 | 5.92 | 4.98 |
| Eu | 0.59 | 0.60 | 0.32 | 0.31 | 1.30 | 1.70 | 1.45 | 1.09 | 1.35 | 1.19 |
| Gd | 1.25 | 1.37 | 1.78 | 2.12 | 4.35 | 5.12 | 4.02 | 2.98 | 3.79 | 2.84 |
| Tb | 0.18 | 0.15 | 0.24 | 0.28 | 0.53 | 0.64 | 0.50 | 0.29 | 0.42 | 0.26 |
| Dy | 0.9 | 0.84 | 1.23 | 1.64 | 2.03 | 2.57 | 2.25 | 1.66 | 2.50 | 1.68 |
| Ho | 0.18 | 0.18 | 0.23 | 0.31 | 0.35 | 0.49 | 0.43 | 0.32 | 0.51 | 0.34 |
| Er | 0.47 | 0.48 | 0.58 | 0.77 | 0.75 | 1.16 | 0.94 | 0.73 | 1.21 | 0.86 |
| Tm | 0.07 | 0.08 | 0.08 | 0.11 | 0.11 | 0.18 | 0.13 | 0.11 | 0.18 | 0.14 |
| Yb | 0.49 | 0.52 | 0.54 | 0.64 | 0.43 | 0.97 | 0.74 | 0.70 | 1.10 | 0.78 |
| Lu | 0.08 | 0.09 | 0.09 | 0.09 | 0.06 | 0.14 | 0.13 | 0.11 | 0.17 | 0.13 |

| | Tiantangzhai | | | | Fuziling | | | | | | |
|---|---|---|---|---|---|---|---|---|---|---|---|
| | 1541-c | 022-1c | H-5 | TS-10T[a] | Z249 | FZL-1[a] | FZL-2-1[a] | FZL-2-2[a] | FZL-2-3[a] | FZ1-2-4[a] | FZL-3[a] |
| $SiO_2$ | 66.80 | 69.82 | 67.09 | 61.8 | 71.01 | 71.05 | 72.11 | 72.46 | 72.63 | 72.62 | 71.58 |
| $TiO_2$ | 0.52 | 0.43 | 0.58 | 0.72 | 0.13 | 0.30 | 0.12 | 0.12 | 0.12 | 0.12 | 0.22 |
| $Al_2O_3$ | 16.42 | 15.43 | 16.04 | 16.31 | 15.40 | 15.14 | 15.13 | 15.13 | 14.91 | 14.97 | 15.01 |
| $Fe_2O_3$ | 1.67 | 1.63 | 1.41 | 4.90 | 0.61 | 0.52 | 0.44 | 0.18 | 0.16 | 0.20 | 0.52 |
| FeO | 1.64 | 1.29 | 1.93 | | 0.55 | 1.03 | 0.48 | 0.68 | 0.63 | 0.77 | 0.75 |
| MnO | 0.03 | 0.04 | 0.05 | 0.04 | 0.01 | 0.01 | 0.01 | 0.01 | 0.01 | 0.01 | 0.01 |
| MgO | 1.17 | 0.35 | 1.60 | 1.26 | 0.51 | 0.44 | 0.27 | 0.25 | 0.25 | 0.27 | 0.33 |
| CaO | 2.35 | 2.29 | 2.63 | 3.20 | 1.28 | 1.55 | 1.31 | 1.04 | 1.16 | 1.10 | 1.29 |
| $Na_2O$ | 4.53 | 4.32 | 4.60 | 5.23 | 4.72 | 4.08 | 5.54 | 4.81 | 5.05 | 4.91 | 3.75 |
| $K_2O$ | 4.61 | 4.25 | 3.83 | 4.87 | 4.60 | 4.98 | 3.78 | 4.47 | 4.24 | 4.23 | 5.56 |
| $P_2O_5$ | 0.26 | 0.16 | 0.23 | 0.32 | 0.05 | 0.06 | 0.03 | 0.03 | 0.03 | 0.02 | 0.04 |
| $H_2O$ | 0.35 | 0.51 | 0.83 | | 0.31 | 0.45 | 0.50 | 0.47 | 0.47 | 0.47 | 0.49 |
| $CO_2$ | 0.04 | 0.03 | 0.11 | 0.74 (LOI) | 0.05 | 0.05 | 0.02 | 0.05 | 0.04 | 0.04 | 0.07 |
| Σ | 100.39 | 100.54 | 100.94 | 99.36 | 99.23 | 99.66 | 99.74 | 99.70 | 99.70 | 99.73 | 99.62 |
| Cr | 21.8 | 11.2 | 29.8 | | 15.5 | 2.13 | 2.75 | 2.83 | 2.90 | 2.59 | 3.65 |
| Ni | 8.1 | 12.2 | 15.3 | 4.88 | 4.0 | 1.89 | 1.44 | 1.43 | 1.89 | 1.48 | 1.78 |
| Co | 8.8 | 4.1 | 10.4 | 7.04 | 3.4 | 2.31 | 0.83 | 0.92 | 0.94 | 0.84 | 1.57 |
| Sc | 5.1 | 1.3 | | 3.05 | | 1.03 | 0.47 | 0.44 | 1.06 | 0.52 | 0.57 |
| V | 45.9 | 47.1 | 58.8 | 81.1 | 14.1 | 15.8 | 4.86 | 6.00 | 6.56 | 7.05 | 10.1 |
| Pb | 22.4 | | 26.4 | 24.8 | 33.6 | 36.0 | 47.2 | 44.0 | 43.0 | 45.1 | 40.6 |
| Rb | 104 | 136 | 105 | 93.0 | 87.5 | 103 | 104 | 81.4 | 91.8 | 93.6 | 98.4 |
| Cs | 3.0 | | | | | 0.412 | 0.358 | 0.232 | 0.244 | 0.250 | 0.288 |
| Ba | 2204 | 1773 | 1963 | 2293 | 1850 | 1718 | 1103 | 922 | 1076 | 1085 | 1814 |
| Sr | 827 | 528 | 732 | 899 | 731 | 830 | 563 | 589 | 567 | 589 | 768 |
| Ga | 22.0 | 21.5 | | 21.2 | | 20.7 | 22.9 | 22.8 | 22.7 | 22.3 | 22.1 |
| Ta | 1.73 | 1.72 | | 0.783 | 0.13 | 0.084 | 0.079 | 0.038 | 0.029 | 0.041 | 0.023 |
| Nb | 14.6 | 12.3 | 11.7 | 12.6 | 2.5 | 3.02 | 1.56 | 1.22 | 1.01 | 1.04 | 1.50 |
| Hf | 7.6 | 3.4 | | 3.40 | 3.6 | 4.23 | 2.05 | 1.43 | 1.95 | 2.09 | 2.53 |
| Zr | 237 | 142 | 219 | 161 | 101 | 152 | 53.6 | 36.3 | 51.9 | 54.2 | 73.5 |
| Y | 13.14 | 11.76 | 13.21 | 13.3 | 0.84 | 1.37 | 0.535 | 0.452 | 0.575 | 0.608 | 0.67 |
| Th | 12.7 | 22.5 | 17.1 | 12.3 | 3.1 | 7.04 | 0.913 | 0.411 | 2.07 | 2.59 | 4.31 |
| U | 2.23 | | | 1.97 | 0.09 | 0.324 | 0.336 | 0.180 | 0.296 | 0.278 | 0.267 |
| La | 74.4 | 44.7 | 71.2 | 61.3 | 15.7 | 25.2 | 5.07 | 6.22 | 8.31 | 9.26 | 18.49 |

(*continued on next page*)

Table 2 (*continued*)

| | Tiantangzhai | | | | Fuziling | | | | | | |
|---|---|---|---|---|---|---|---|---|---|---|---|
| | 1541-c | 022-1c | H-5 | TS-10T[a] | Z249 | FZL-1[a] | FZL-2-1[a] | FZL-2-2[a] | FZL-2-3[a] | FZ1-2-4[a] | FZL-3[a] |
| Ce | 139 | 81.4 | 122 | 102 | 26.5 | 45.8 | 8.18 | 10.4 | 14.5 | 16.8 | 31.3 |
| Pr | 15.3 | 10.1 | 12.4 | 12.1 | 2.98 | 5.01 | 0.968 | 1.19 | 1.67 | 1.91 | 3.50 |
| Nd | 50.1 | 31.7 | 40.8 | 42.6 | 8.25 | 16.57 | 3.40 | 4.03 | 5.93 | 6.76 | 11.9 |
| Sm | 7.37 | 5.28 | 5.88 | 6.81 | 1.07 | 2.17 | 0.534 | 0.628 | 0.822 | 0.934 | 1.45 |
| Eu | 1.74 | 1.28 | 1.41 | *1.71* | 0.520 | 0.682 | 0.412 | 0.385 | 0.352 | 0.376 | 0.669 |
| Gd | 4.72 | 3.74 | 3.95 | 4.55 | 0.61 | 0.903 | 0.295 | 0.289 | 0.297 | 0.323 | 0.529 |
| Tb | 0.51 | 0.44 | 0.40 | 0.619 | 0.05 | 0.099 | 0.031 | 0.032 | 0.035 | 0.037 | 0.055 |
| Dy | 2.79 | 2.48 | 2.59 | 2.92 | 0.210 | 0.337 | 0.114 | 0.109 | 0.164 | 0.159 | 0.162 |
| Ho | 0.52 | 0.46 | 0.49 | 0.489 | 0.039 | 0.046 | 0.017 | 0.014 | 0.022 | 0.022 | 0.022 |
| Er | 1.17 | 1.18 | 1.22 | 1.22 | 0.090 | 0.116 | 0.044 | 0.037 | 0.044 | 0.051 | 0.052 |
| Tm | 0.17 | 0.16 | 0.18 | 0.175 | 0.010 | 0.016 | 0.007 | 0.005 | 0.006 | 0.007 | 0.007 |
| Yb | 1.01 | 1.23 | 1.15 | 1.31 | 0.067 | 0.088 | 0.042 | 0.0330 | 0.046 | 0.044 | 0.046 |
| Lu | 0.16 | 0.17 | 0.13 | 0.216 | 0.010 | 0.017 | 0.008 | 0.005 | 0.009 | 0.008 | 0.008 |

| | Fuziling FZL-3* (Re) | Dikes | | | | | | Baiyashan | | Int. granite standard | |
|---|---|---|---|---|---|---|---|---|---|---|---|
| | | 2028-2c | 2087-2c | 1001-3 | 1651-3 | YFD-7[a] | EGB-6[a] | B1-2 | b11-2 | G-2 | G-2(RV) |
| $SiO_2$ | | 72.26 | 72.75 | 72.77 | 71.12 | 72.66 | 72.84 | 73.6 | 70.12 | | |
| $TiO_2$ | | 0.29 | 0.24 | 0.13 | 0.36 | 0.28 | 0.28 | 0.2 | 0.38 | | |
| $Al_2O_3$ | | 14.08 | 13.65 | 14.20 | 14.04 | 13.81 | 13.58 | 14.05 | 15.17 | | |
| $Fe_2O_3$ | | 0.99 | 0.90 | 0.74 | 1.27 | 0.77 | 0.69 | 0.81 | 1.04 | | |
| FeO | | 0.91 | 0.83 | 0.82 | 1.00 | 1.22 | 1.28 | 0.64 | 1.4 | | |
| MnO | | 0.04 | 0.02 | 0.02 | 0.03 | 0.05 | 0.05 | 0.04 | 0.06 | | |
| MgO | | 0.62 | 0.54 | 0.25 | 0.52 | 0.50 | 0.45 | 0.22 | 0.46 | | |
| CaO | | 1.32 | 1.18 | 1.54 | 1.68 | 1.39 | 1.28 | 1.18 | 1.92 | | |
| $Na_2O$ | | 3.71 | 3.62 | 3.85 | 3.70 | 3.51 | 3.46 | 3.5 | 3.62 | | |
| $K_2O$ | | 4.66 | 4.70 | 4.48 | 5.08 | 4.87 | 5.10 | 4.66 | 4.86 | | |
| $P_2O_5$ | | 0.08 | 0.05 | 0.06 | 0.10 | 0.06 | 0.06 | 0.05 | 0.14 | | |
| $H_2O$ | | 0.68 | 0.46 | 0.56 | 0.48 | 0.57 | 0.60 | 0.51 | 0.47 | | |
| $CO_2$ | | 0.07 | 0.08 | 0.02 | 0.00 | 0.09 | 0.12 | 0.29 | 0.12 | | |
| Σ | | 99.71 | 99.02 | 99.44 | 99.38 | 99.78 | 99.79 | 99.75 | 99.76 | | |
| Cr | 5.28 | 18.1 | 14.0 | 4.0 | 11.0 | 7.20 | 8.00 | 13.1 | 12.2 | 8.84 | 8.7 |
| Ni | 1.48 | 3.00 | 4.00 | 2.0 | 2.3 | 3.53 | 3.36 | 5.5 | 8.6 | 5.45 | 5 |
| Co | 1.58 | 3.80 | 4.00 | 3.0 | 4.0 | 2.38 | 2.42 | | | 4.50 | 4.6 |
| Sc | 0.58 | | | | | 3.15 | 4.33 | 3.5 | 4.3 | 3.49 | 3.5 |
| V | 9.64 | 22.0 | 19.0 | 16.0 | 23.9 | 18.7 | 16.1 | | | 36.3 | 36 |
| Pb | 41.3 | 26.0 | 25.0 | 41.0 | 28.0 | 26.6 | 28.7 | | | 31.2 | 30 |
| Rb | 97.6 | 209 | 221 | 228 | 193 | 181 | 218 | 260 | 936 | 171 | 170 |
| Cs | 0.284 | | | | | 1.89 | 1.79 | | | 1.38 | 1.34 |
| Ba | 1877 | 870 | 728 | 724 | 1529 | 863 | 938 | 582 | 287 | 1894 | 1882 |
| Sr | 794 | 218 | 161 | 156 | 236 | 253 | 224 | 122 | 217 | 491 | 478 |
| Ga | 22.6 | | 22.0 | 25.0 | | 17.8 | 19.5 | | | 22.7 | 23 |
| Ta | 0.021 | | 3.50 | 2.29 | | 0.955 | 1.29 | 2.6 | 3.1 | 0.870 | 0.88 |
| Nb | 1.50 | 21.2 | 18.6 | 18.7 | 20.0 | 14.83 | 18.64 | 22.1 | 29.8 | 11.9 | 12 |
| Hf | 2.56 | | 6.0 | 4.3 | | 5.36 | 6.65 | 5.3 | 6.7 | 7.79 | 7.9 |
| Zr | 72.8 | 218 | 169 | 167 | 333 | 181 | 222 | 167 | 249 | 308 | 309 |
| Y | 0.68 | 27.8 | 27.0 | 14.0 | 26.5 | 20.9 | 31.4 | 35.3 | 36.1 | 9.76 | 11 |
| Th | 4.43 | 19.2 | 17.4 | 16.7 | 29.4 | 27.1 | 34.8 | 18.2 | 21.5 | 24.4 | 24.7 |
| U | 0.328 | | | | | 2.85 | 3.90 | 7.54 | 3.40 | 1.89 | 2.07 |
| La | 18.17 | 59.2 | 50.9 | 42.7 | 108 | 65.1 | 87.7 | 57.4 | 78.2 | 89.6 | 89 |
| Ce | 30.6 | 113 | 97.2 | 77.5 | 197 | 127 | 170 | 100 | 139 | 161 | 160 |
| Pr | 3.38 | 12.2 | 10.3 | 8.85 | 21.0 | 13.3 | 18.0 | 11.7 | 16.3 | 16.9 | 18 |
| Nd | 11.5 | 40.3 | 33.4 | 26.7 | 67.7 | 42.9 | 58.9 | 42.8 | 56.6 | 58.5 | 55 |
| Sm | 1.42 | 6.86 | 5.80 | 5.05 | 9.68 | 6.33 | 8.60 | 7.28 | 9.25 | 7.25 | 7.2 |
| Eu | 0.678 | 0.859 | 0.640 | 0.718 | 1.14 | 0.704 | 0.852 | 0.76 | 1.26 | 1.30 | 1.4 |
| Gd | 0.552 | 5.17 | 4.75 | 3.88 | 6.54 | 3.841 | 5.341 | 6.0 | 7.08 | 4.46 | 4.3 |
| Tb | 0.052 | 0.72 | 0.71 | 0.56 | 0.77 | 0.656 | 0.954 | 1.03 | 1.16 | 0.52 | 0.48 |
| Dy | 0.164 | 4.57 | 4.65 | 2.86 | 5.15 | 3.50 | 5.20 | 5.7 | 6.19 | 2.26 | 2.4 |
| Ho | 0.022 | 0.92 | 0.92 | 0.53 | 0.98 | 0.670 | 1.00 | 1.12 | 1.26 | 0.364 | 0.4 |
| Er | 0.055 | 2.56 | 2.59 | 1.39 | 2.53 | 1.91 | 2.90 | 3.33 | 3.69 | 1.02 | 0.92 |
| Tm | 0.008 | 0.42 | 0.41 | 0.21 | 0.38 | 0.285 | 0.462 | 0.54 | 0.61 | 0.122 | 0.18 |

Table 2 (*continued*)

| | Fuziling FZL-3* (Re) | Dikes | | | | | | Baiyashan | | Int. granite standard | |
|---|---|---|---|---|---|---|---|---|---|---|---|
| | | 2028-2c | 2087-2c | 1001-3 | 1651-3 | YFD-7[a] | EGB-6[a] | B1-2 | b11-2 | G-2 | G-2(RV) |
| Yb | 0.050 | 2.77 | 2.51 | 1.19 | 2.25 | 1.92 | 3.12 | 3.59 | 3.87 | 0.714 | 0.8 |
| Lu | 0.010 | 0.44 | 0.39 | 0.17 | 0.33 | 0.312 | 0.503 | 0.53 | 0.58 | 0.110 | 0.11 |

Data of the Baiyashan granites are after Ma et al. (1998), other data are from this study. Re, repeated; RV, recommended values.
[a] Analysed by ICP-MS, others by ICP-AES.

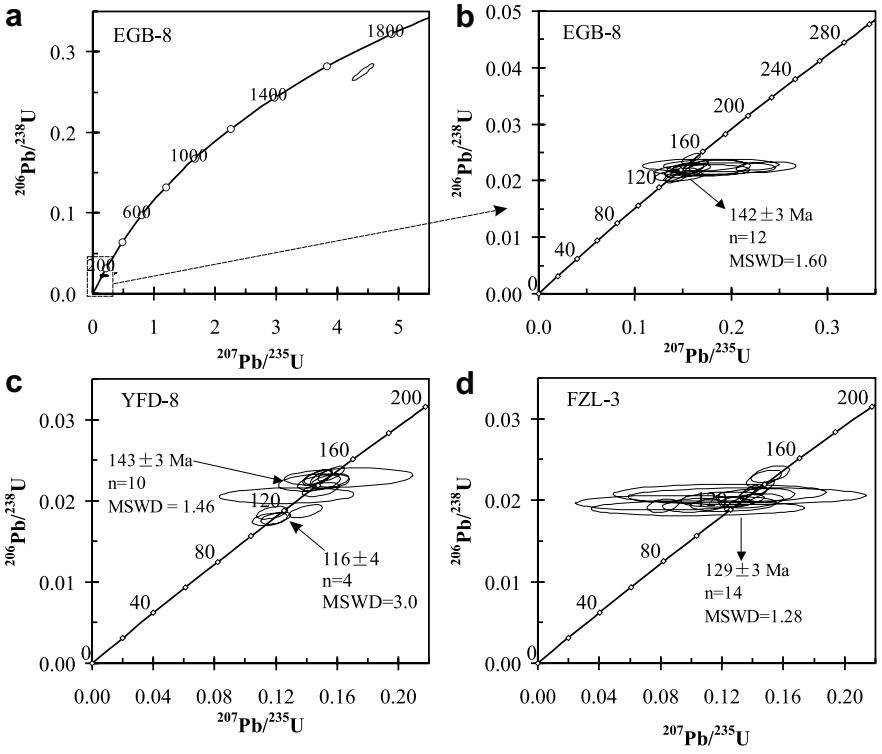


Fig. 2. SHRIMP zircon U–Pb concordia diagrams for samples EGB-8 (Egongbao) (a,b), YFD-8 (Yunfengding) (c), and FZL-3 (Fuziling) (d).

Wang et al. (1998) reported a zircon U–Pb age of 131.3 ± 4.0 Ma for the early Tiantangzhai intrusion. Thus, the main early granite intrusions in the study area formed between 143 and 129 Ma. Given the range of previously published age data of Cretaceous granites (137–94 Ma: e.g., Hacker et al., 1998; Bryant et al., 2004) and mafic–ultramafic intrusive rocks (130–123 Ma: e.g., Jahn et al., 1999; Zhao et al., 2005) in the Dabie Orogen (Fig. 1b), we suggest that the Egongbao and Yunfengding granites (142–143 Ma) are the oldest of all Cretaceous intrusive rocks in this area. The associated granitic dikes, however, exhibit geological and petrographic characteristics similar to the late (118–105 Ma) granites in the NDC, and have similar geochemical characteristics, as discussed below. Accordingly, we infer that the dikes and late granites (the Bamajian, Zhuboyuan, and Baiyashan intrusions) were products of approximately contemporaneous magmatism.

### 5.2. Major and trace-element geochemistry

The major and trace element compositional characteristics and classification of the granites in the study area are shown in Figs. 3 and 4a. Fields of Cretaceous (130–123 Ma) pyroxenites and gabbros in the Dabie Orogen are also plotted in Figs. 3 and 4. Apart from several samples in the trondhjemite field, all of the Cretaceous intrusions plot in the granite field in the Albite–Anorthite–Orthoclase diagram (Fig. 3a). Most samples plot in the medium-Fe field (Fig. 3b) and high-K field (Fig. 4a) of igneous rocks, in contrast to slab-derived adakites in the low-Fe and middle- and low-K fields (Fig. 2 of Wang et al. (2004a)). Almost all samples plot near the boundary between metaluminous and peraluminous compositions (ACNK ($Al_2O_3$/(CaO + $Na_2O$ + $K_2O$)) = 0.91–1.04) (Fig. 3c). The late dikes define fields similar to those of the four granites on major element Harker diagrams (Figs. 4 and 5),

which are separated from the fields of mafic–ultramafic samples by a distinct compositional gap in silica contents between $SiO_2 = 56\%$ and 64%. On trace element plots, however, the early granitoids clearly display higher Sr (Fig. 5b) but lower Th, Rb, Y and Yb (Fig. 5c–f) contents than the late dikes.

Chondrite-normalized REE and N-MORB normalized trace element patterns (Fig. 6) show that all sampled granites and dikes are enriched in light REE (LREE) and depleted in Nb, Ta, and Ti. However, the granites exhibit strong depletion in heavy REE (HREE) (Fig. 6a, c, and e) and negligible to positive Eu and Sr and positive Ba anomalies, except for Tiantangzai granites samples 1648 and H14, which clearly shows negative Eu anomalies. Apart from these two samples, the early Egongbao, Yufengding, and Tiantangzai granites display REE and trace element patterns which are distinct from those of the late granites (Ma et al., 1998; Chen et al., 2002; Bryant et al., 2004) but similar to slab-derived adakites (e.g., Defant and Drummond, 1990; Kay et al., 1993; Stern and Kilian, 1996; Aguillón-Robles et al., 2001; Martin et al., 2005) (Fig. 6a–d). The Fuziling granite samples are notable for their clearly positive Eu and Sr anomalies, extraordinarily high Sr/Y (607–1303) and La/Yb (121–402) ratios (Fig. 7a and b, and Table 2), and depletions in HREE that are much lower than even those of slab-derived adakites (Fig. 6e and f). In contrast, the granitic dikes exhibit clearly negative Eu and Sr anomalies and no fractionation between the MREE and HREE, which is similar to the late granites (Ma et al., 1998; Chen et al., 2002; Bryant et al., 2004) (Fig. 6e and f). These distinctions are emphasized on Sr/Y versus Y and $(La/Yb)_N$ versus $Yb_N$ diagrams (Fig. 7a and b) where the early granites plot in the adakite field, but most of the late dikes and granites fall in the "normal" andesite–dacite–rhyolite field.

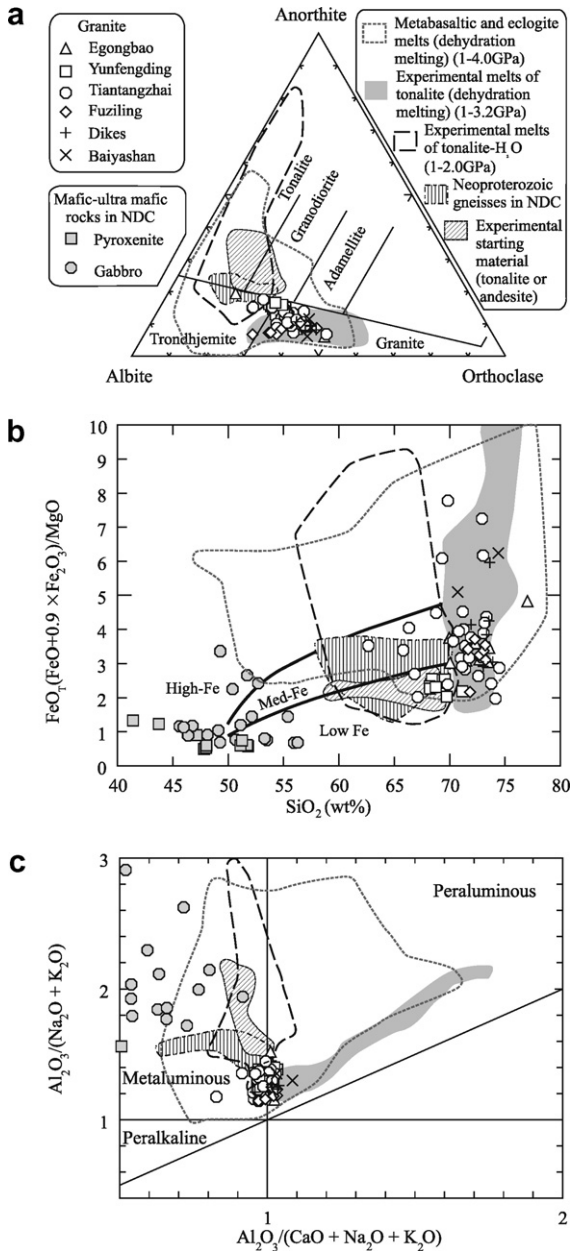


Fig. 3. (a) Albite–Anorthite–Orthoclase diagram of the Cretaceous granites in the Jiuzihe–Zhangjiazui area. (b) $SiO_2$ versus $FeO_T$ $(FeO + 0.9Fe_2O_3)/MgO$ diagram. The discriminant boundaries (bold lines) between low-, medium-, and high-Fe igneous rocks suites are from Arculus (2003). (c) $Al_2O_3/(CaO + Na_2O + K_2O)$ versus $Al_2O_3/(Na_2O + K_2O)$ diagram. The field of metabasaltic and eclogite melts (dehydration melting) (1–4.0 GPa) is constructed using data from the following: Sen and Dunn (1994); Rapp and Watson (1995); Rapp et al. (1999, 2002, 2003); Skjerlie and Patiño Douce (2002), and references therein. The field of experimental melts of tonalite–$H_2O$ (1–2.0 GPa) is constructed using data from the following: Carroll and Wyllie, 1989, 1990, and references therein. The field of experimental melts of tonalite (dehydration melting) (1–3.2 GPa) is constructed using data from the following: Skjerlie and Johnston (1993); Patiño Douce and McCarthy (1998); Patiño Douce (2005), and references therein. The field of experimental starting material (tonalite or andesite) is constructed using data from the following: Skjerlie and Johnston (1993); Patiño Douce and McCarthy (1998); Carroll and Wyllie (1989, 1990); Patiño Douce (2005), and references therein. The data of Cretaceous mafic–ultramafic intrusive rocks in the Dabie area are from Jahn et al. (1999), Wang and Deng (2002), and Zhao et al. (2005). The data of Neoproterozoic gneisses in the northern Dabie Orogen and the Baiyashan granites are from Ma et al. (1998) and Bryant et al. (2004), respectively. The data of the granites in the Jiuzihe–Zhangjiazui area are from Li and Wang (1991) and Table 2.

### 5.3. Nd and Sr isotopes

The early adakitic granites in the study area have relatively homogeneous $\varepsilon_{Nd}(t)$ values ranging from −14.6 to −19.4, and $(^{87}Sr/^{86}Sr)_i$ (initial $^{87}Sr/^{86}Sr$) ratios ranging from 0.7067 to 0.7087 (Table 3). These isotopic characteristics are clearly different from those of Cenozoic slab-derived adakites ($\varepsilon_{Nd} > +6.0$; $(^{87}Sr/^{86}Sr)_i < 0.7045$) (Defant et al., 1992; Kay et al., 1993; Aguillón-Robles et al., 2001) and late Mesozoic delaminated lower crust-derived adakitic rocks in the eastern Yangtze Block ($\varepsilon_{Nd} = -9.7$ to $+1.8$; $(^{87}Sr/^{86}Sr)_i = 0.7044$–$0.7073$) (Xu et al., 2002; Wang et al., 2004a,b, 2006a,b), but are similar to that of thickened lower crust-derived adakitic granites in the eastern Yangtze Block ($\varepsilon_{Nd} = -18.1$ to $-17.0$; $(^{87}Sr/^{86}Sr)_i = 0.7071$–$0.7072$) (e.g., Hongzhen area; Fig. 1a: Wang et al., 2004a; Fig. 8). In the $\varepsilon_{Nd}(t)$ versus $(^{87}Sr/^{86}Sr)_i$ diagram (Fig. 8), samples of

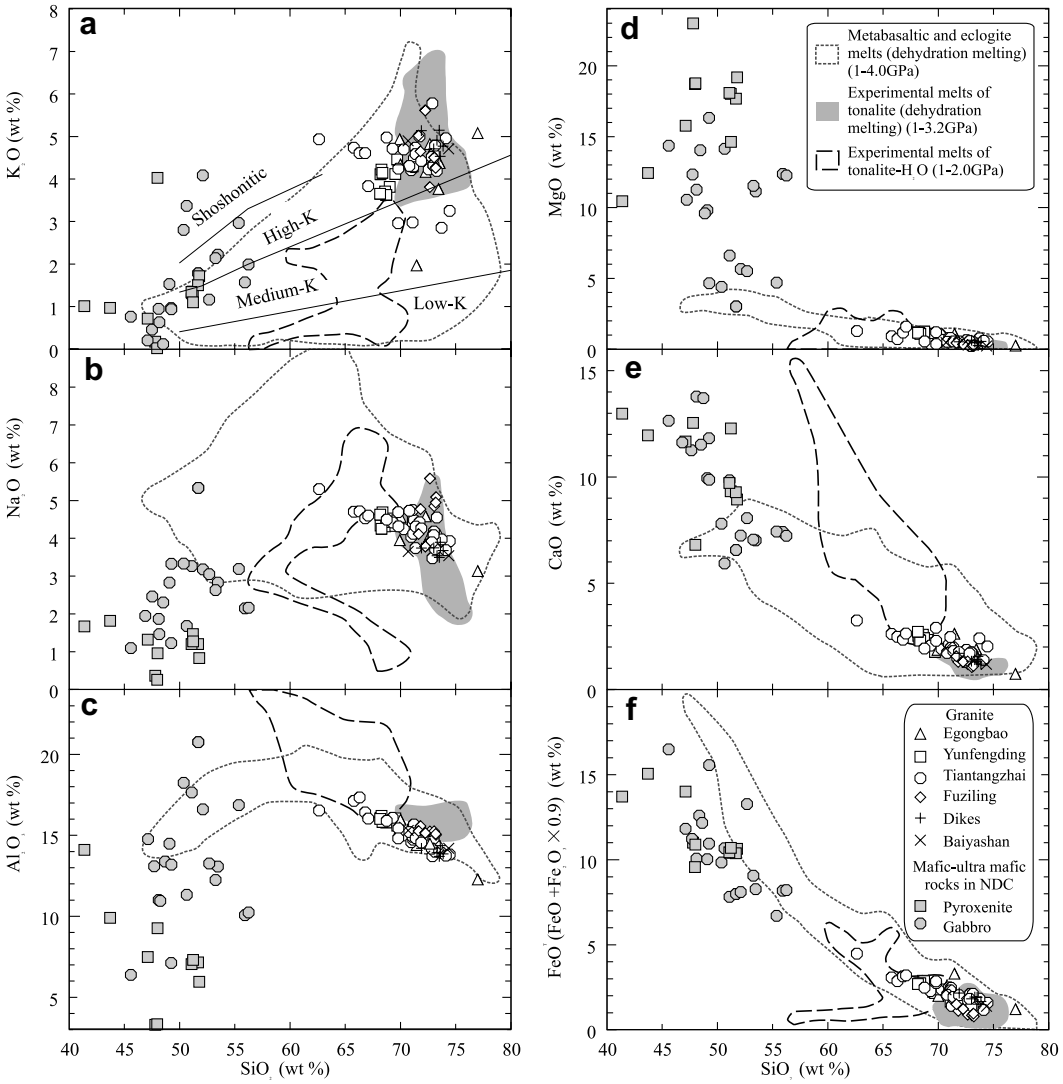


Fig. 4. Harker variation diagrams showing the major element variations of the granites in the Jiuzihe–Zhangjiazui area and mafic–ultramafic rocks in the Dabie area. The fields of metabasaltic and eclogite melts (dehydration melting) (1–4.0 GPa), experimental melts of tonalite–$H_2O$ (1–2.0 GPa), experimental melts of tonalite (dehydration melting) (1–3.2 GPa), and Cretaceous mafic–ultramafic intrusive rocks are constructed using the same data sources as in Fig. 3. The data of the granites in the Jiuzihe–Zhangjiazui area are from the same data sources as in Fig. 3.

the early granites plot in or near to the fields of Cretaceous mafic–ultramafic intrusive rocks in the Dabie, but are distinct from the field of Neoproterozoic (700–800 Ma) orthogneisses and amphibolites (e.g., Bryant et al., 2004; Figs. 8 and 9). The granite dikes and the late Baimajian and Zhuboyuan granites located east of the study area (Fig. 1b) have similar isotopic compositions but are displaced to slightly more negative $\varepsilon_{Nd}(t)$ values than the four early granites. Only the late Baiyashan intrusion to the west of the study area (Fig. 1b) exhibits lower $\varepsilon_{Nd}(t)$ and distinctly higher $(^{87}Sr/^{86}Sr)_i$ than the adakitic granites (Fig. 8).

## 6. DISCUSSION

### 6.1. Potassium and the adakite classification

The early granites described here from the Jiuzhihe–Zhangjiazui area of the NDC clearly fall within the adakite field on commonly used discrimination diagrams such as the Sr versus Y plot and the $(La/Yb)_N$ versus Yb plot illustrated in Fig. 7. In addition, they plot in the field of metabasalt and eclogite melting (Fig. 3). An important question then, is whether these rocks should be classified as adakites or whether their K contents represent the grounds for an a priori disqualification from the adakite classification. While trondhjemites and sodic rhyolites were described as a common components of adakite suites in the Defant and Drummond (1990) paper that introduced the term, these authors did not list Na contents as a defining characteristic of the adakites, which were classified on the basis of Y, Yb, Sr/Y, Si, Al, and Mg contents. We argue that the term is appropriate here on the basis of sound petrological practice and precedence.

First, the notion that adakites are only derived from subducted metabasaltic sources, and therefore are consistently K-poor, is contrary to the general concept that petrological

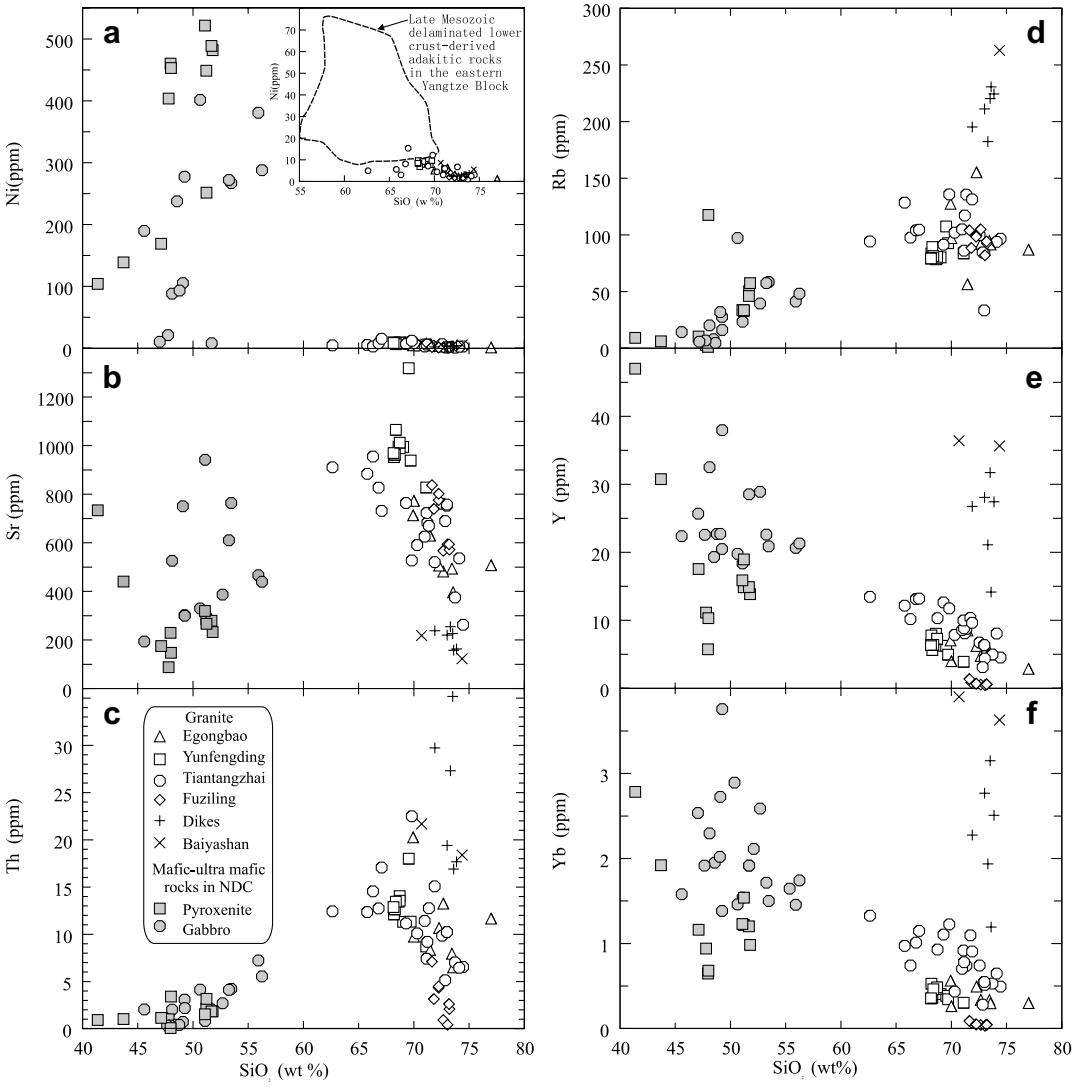


Fig. 5. Harker variation diagrams showing the trace element variations of the granites in the Jiuzihe–Zhangjiazui area. The fields of Late Mesozoic delaminated lower crust-derived adakitic rocks in the eastern Yangtze Block are constructed using data from the following: Xu et al. (2002) and Wang et al. (2004a,b, 2006a,b). The data of the granites in the Jiuzihe–Zhangjiazui area are from the same data sources as in Fig. 3.

definitions should be independent of genetic theories that could be subsequently disproved. The evolving concepts associated with A-type granites or boninites illustrate the pitfalls of linking a genetic interpretation to a rock type definition. At very least, a restrictive characterization of adakites as the K-poor products slab melting could fail to accommodate natural variations in mainly slab-derived adakite compositions that might arise from sediments on the slab or interaction with continental crust. More generally, many reviews of adakites explicitly acknowledged the possibility of sources other than subducted basaltic crust. For example, Kay and Kay (2002) suggest that Andean adakites may be generated by tectonic thickening of Andean crust or subduction erosion of fore-arc crust as well by subduction of young oceanic crust. Defant et al. (2002) also included lower crustal delamination as a possible mechanism for adakite formation and noted that, if this process occurred then "the term adakite should not be restricted to processes related only to slab melting but must include those involving the melting of the lower crust" (p. 129). Many other workers such as Harris et al. (1996), Arculus et al. (1999), Rapp et al. (2002), Gao et al. (2004), and Castillo (2006) have suggested that certain lower-crust derived rocks can properly be termed adakites, adakite-like or adakitic.

Second, some K-rich rocks have already been described as "adakitic". For example, the well known high-K–calc alkaline Cordillera Blanca granodiorites, inferred by Atherton and Petford (1993) and Petford and Atherton (1996) to be derived by underplating of new lower crust, were subsequently characterized as adakites by Gutscher et al. (2000) and others. Some Cenozoic granitic rocks in Tibet and the Andes have $K_2O$ (4.35–8.56 wt%) and $K_2O/Na_2O$ ratios (1.63–3.71) that are far higher than those of the study area (2.94–5.74 wt%; 0.63–1.64) and have been termed "adakitic rocks" (Chung et al., 2003; Hou et al., 2004; Qu et al., 2004; Kay et al., 2005). Similarly, the compilation of adakite data

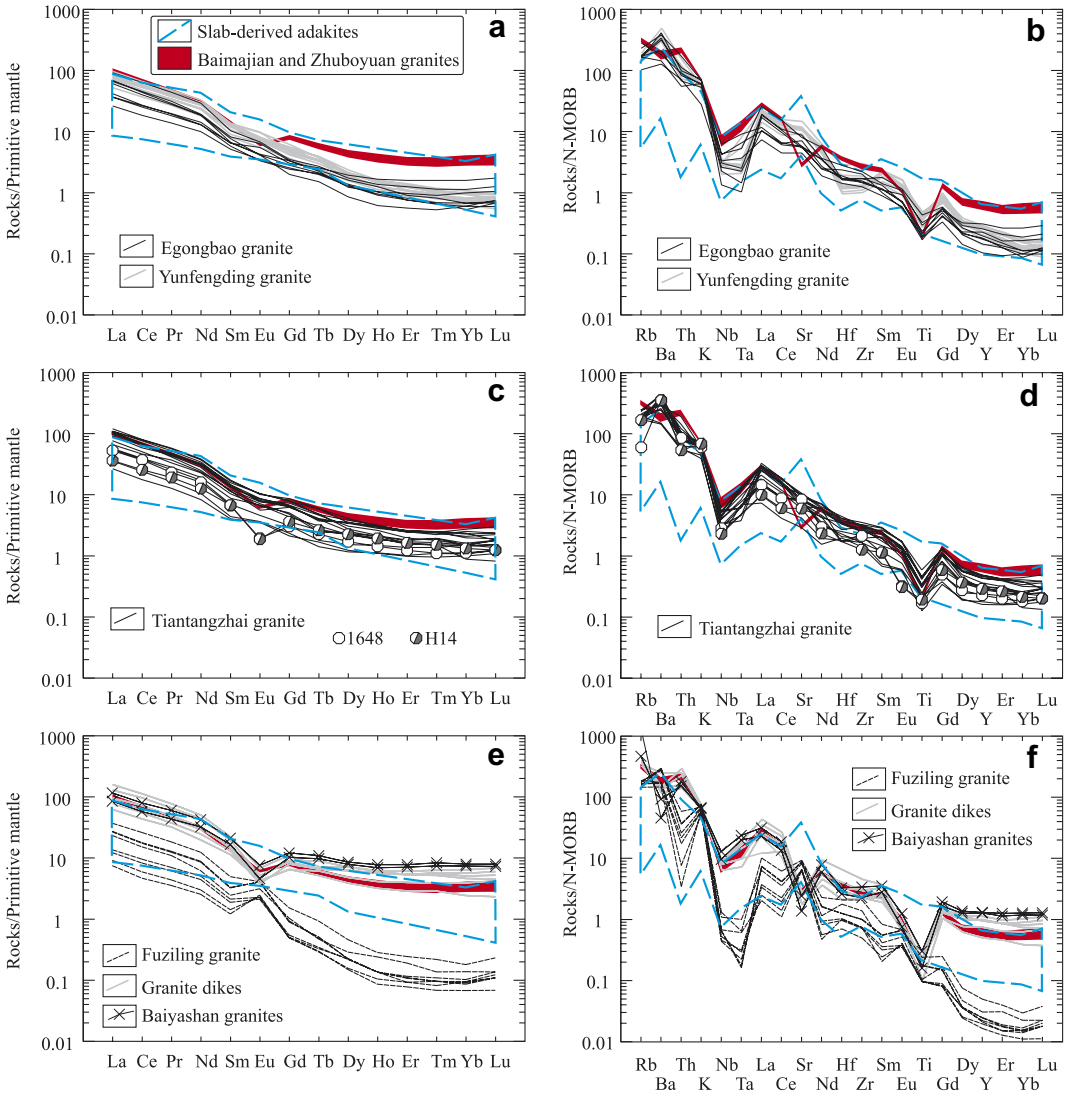


Fig. 6. Primitive mantle normalized rare earth element (REE) patterns and N-MORB normalized multi-element profiles of the granites in the Jiuzihe–Zhangjiazui area. Primitive mantle and N-MORB normalizing values are from Sun and McDonough (1989). (a) REE patterns of the Egongbao and Yunfengding adakitic granites. (b) Multi-element profiles of the Egongbao and Yunfengding adakitic granites. (c) REE patterns of the Tiantangzhai adakitic granites. (d) Multi-element profiles of the Tiantangzhai adakitic granites. (e) REE patterns of the granitic dikes in the Jiuzihe–Zhangjiazui area and the Fuziling adakitic granites. (f) Multi-element profiles of the granitic dikes in the Jiuzihe–Zhangjiazui area, the Fuziling adakitic granites and the Baiyashang granites. The REE and trace element data for the Baiyashan, Zhuboyuan, and Baimajian granites are from Ma et al. (1998), Chen et al. (2002), and Bryant et al. (2004). The REE and trace element data of subducted oceanic crust-derived adakites are from Defant and Drummond (1990), Kay and Kay (1993), Stern and Kilian (1996), Aguillón-Robles et al. (2001), Defant et al. (2002), Martin et al., 2005, and references therein. The data of the granites in the Jiuzihe–Zhangjiazui area are from the same data sources as in Fig. 3.

presented by Martin et al. (2005) includes a plot of adakite K content that extends beyond 35,000 ppm (4.2 wt% $K_2O$). In addition, Rapp et al. (2002) described some high-K–calc alkaline igneous rocks from eastern China as "potassium-rich adakites" and Xiao and Clemens (2007) refer to the Tianntangzhai granite of the Dabie area as "potassic adakite".

In summary, the use of the term "adakite" or "adakitic" for the early granites of the NDC study area is consistent with their conformity to key discrimination criteria, with current usage of the terms, and emphasizes petrogenetic comparisons with the most relevant igneous rock types world-wide.

### 6.2. Petrogenesis of the adakitic granites in the NDC

On the basis of the tectonic setting, geochemical characteristics, and zircon dating, three commonly invoked models of adakite genesis (slab melting, assimilation and fractional crystallization process (AFC), and melting of delaminated lower crust) appear to be untenable explanations for the adakitic granites in the NDC. We first discuss the

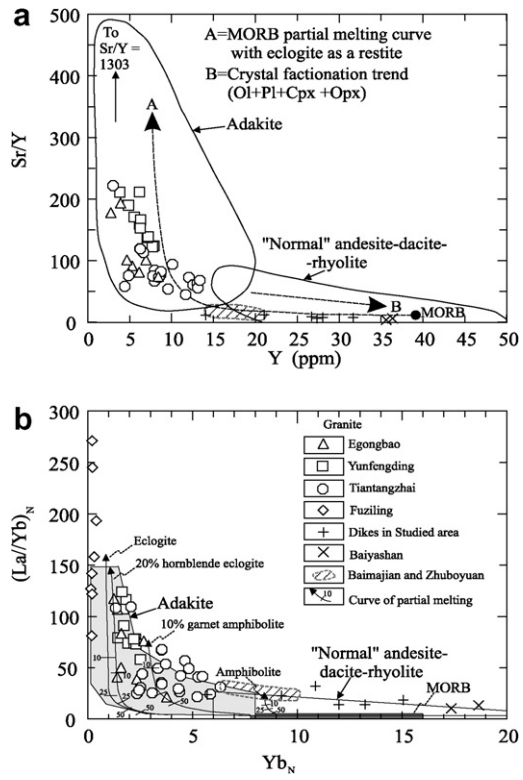


Fig. 7. (a) Sr/Y versus Y (after Defant et al. (2002)); (b) $La_N/Yb_N$ versus $Yb_N$ diagram (after Drummond and Defant (1990)). Ol, olivine; Pl, plagioclase; Cpx, clinopyroxene; Opx, orthopyroxene. The data for the Zhuboyuan, Baimajian, and Baimajian granites are from the same data sources as in Fig. 6. The data of the granites in the Jiuzihe–Zhangjiazui area are from the same data sources as in Fig. 3.

weaknesses of these models and then focus in more detail on partial melting of thickened lower crust as a mechanism for generation of the adakitic rocks.

*6.2.1. Models 1–3: slab melting, AFC processs, and melting of delaminated lower crust*

The adakitic early granites in the study area occur in the core of a contemporaneous metamorphic core complex (i.e., NDC), which resulted from 100% crustal stretching of a pre-existing ~245 Ma collisional crustal architecture (Hacker et al., 1998) in an interior continental setting (Fig. 1a and b). This association argues strongly against any Cretaceous subduction in this area. In addition, the adakitic granites have extraordinarily low $\varepsilon Nd(t)$ and relatively high initial $^{87}Sr/^{86}Sr$ isotopic compositions (Fig. 8; Table 3) that are improbable for granitic melts produced by partial melting of subducted oceanic crust in the Cretaceous. Their very low compatible element abundances (e.g., Ni: Fig. 5a) and $Mg^{\#}$ values (Fig. 10) are also not consistent with melts that have traversed mantle peridotites in either (a) a wedge above a subducting slab or (b) the gap created above delaminated and melting lower crust (Xu et al., 2002; Gao et al., 2004; Wang et al., 2004a,b, 2006a,b).

Two Tiantanzhai granite samples (1648 and H14) have negative Eu anomalies, probably resulting from the fractional crystallization of minor plagioclase (Fig. 6c). All other adakitic granite samples exhibit either no Eu and Sr anomalies or positive anomalies (Fig. 6), arguing against a significant role for plagioclase fractional crystallization in their genesis (Wilson, 1989). Ma et al. (1998) suggested that AFC processes could only be responsible for Cretaceous Y- and Yb-depleted and $Al_2O_3$- and Sr-enriched granites in the Dabie area if amphibole fractionation had taken place. However, the adakitic granites in the study area lack any obvious depletion in middle REE (Fig. 6), suggesting that amphibole fractionation did not play an important role in their petrogenesis (Gromet and Silver, 1987). In addition, the adakitic granites lack clear compositional trends indicative of fractional crystallization from Cretaceous mafic–ultramafic magmas in the Dabie Orogen (Figs. 4, 5, 7a, 10, and 11a) and there is a compositional gap (e.g., $SiO_2$: 55–62 wt%) between the granites and mafic–ultramafic rocks (Figs. 4 and 5), suggesting that the fractional crystallization could not be main factor responsible for compositional variation of the early granites (e.g., Castillo et al., 1999). Moreover, the mafic–ultramafic intrusive rocks formed at 130–123 Ma and postdated the earliest adakitic granites (e.g., the 143–142 Ma Yunfengding and Egongbao granites), ruling out a genetic link. The mafic–ultramafic intrusive rocks were contemporaneous with the 131–129 Ma Tiangtangzhai and Fuziling adakitic granites, but there is nothing to suggest that Tiangtangzhai formed by different mechanisms than the 143–142 Ma intrusions, apart from some minor fractionation documented in two samples. The size of the Tiantangzhai intrusion (400 $km^2$) also suggests that it could not be produced solely by AFC processes. The Fuziling intrusion has an outcrop area of only about 1.8 $km^2$, but its distinctive geochemical characteristics (e.g., strongly positive Eu and Sr anomalies) argue against fractional crystallization involving plagioclase and hornblende from mafic–ultramafic magmas.

*6.2.2. Model 4: partial melting of thickened lower crust*

The early NDC adakitic granites display compositional trends consistent with partial melting (Figs. 11a), suggesting that this process was responsible for their petrogenesis. Chen and Jahn (1998) suggested that Cretaceous granites in the NDC were derived from remelting of old (Mid-Proterozoic) continental crust, probably at a lower crustal level. Zhang et al. (2002a) suggested that all Cretaceous granites were derived by partial melting of a source similar to the Proterozoic gneisses and amphibolites in the NDC. Zhao et al. (2005) argued that partial melting of the thickened (or subducted) and sandwich-structured mafic–ultramafic and felsic layers of Neoproterozoic ages beneath the collisional orogen was a viable mechanism for genesis of the Cretaceous mafic–ultramafic and granitic intrusive rocks, respectively. New geochemical and isotopic data show, however, that the NDC Neoproterozoic (700–800 Ma) gneisses and amhibolites have distinct Nd isotope composition and therefore could not generate the Cretaceous granites via partial melting (Bryant et al., 2004) (Figs. 8 and 9).

Table 3
Sr–d isotopic compositions for the adakitic granites and late dikes in the Northern Dabie Complex

| Intrusion | Rock type | Sample | Sm (ppm) | Nd (ppm) | $^{147}Sm/^{144}Nd$ | $^{143}Nd/^{144}Nd$ | $2s_m$ | $T$ (Ma) | $(^{143}Nd/^{144}Nd)_i$ | $f_{Sm/Nd}$ | $\varepsilon ND(t)$ | $T_{DM}$ (Ga) | Rb (ppm) | Sr (ppm) | $^{87}Rb/^{86}Sr$ | $^{87}Sr/^{86}Sr$ | $2s_m$ | $(^{87}Sr/^{86}Sr)_i$ | References |
|---|---|---|---|---|---|---|---|---|---|---|---|---|---|---|---|---|---|---|---|
| Tiantangzhai | AG | 116 | | | 0.107 | 0.511617 | 10 | 2.18 | 0.511525 | −0.46 | −18.4 | 2.18 | | | 0.4378 | 0.70855 | 6 | 0.7077 | Ma et al. (1998) |
| | AG | 117 | | | 0.0914 | 0.511688 | 19 | 1.82 | 0.511610 | −0.54 | −16.8 | 1.82 | | | 0.5268 | 0.70875 | 1 | 0.7078 | Ma et al. (1998) |
| | AG | JZ34 | | | 0.0949 | 0.511665 | 8 | 1.90 | 0.511584 | −0.52 | −17.3 | 1.90 | | | 0.6981 | 0.70804 | 4 | 0.7067 | Ma et al. (2000) |
| | AG | H-5 | 6.493 | 40.42 | 0.1012 | 0.511560 | 9 | 2.15 | 0.511473 | −0.49 | −19.4 | 2.15 | 99.85 | 791.9 | 0.3558 | 0.707960 | 39 | 0.7073 | This study |
| | AG | 1648-1 | 4.837 | 31.34 | 0.0973 | 0.511734 | 8 | 1.85 | 0.511651 | −0.51 | −16.0 | 1.85 | 94.30 | 762.6 | 0.3490 | 0.708661 | 47 | 0.7080 | This study |
| Fuziling | AG | FZL-1 | 1.972 | 14.54 | 0.08202 | 0.511645 | 2 | 1.74 | 0.511576 | −0.58 | −17.5 | 1.74 | 104.6 | 863.4 | 0.3506 | 0.708710 | 5 | 0.7081 | This study |
| | AG | FZL-2-1 | 0.5564 | 3.65 | 0.09221 | 0.511693 | 12 | 1.82 | 0.511615 | −0.53 | −16.7 | 1.82 | 82.29 | 609.4 | 0.3910 | 0.708972 | 10 | 0.7083 | This study |
| | AG | FZL-3 | 1.433 | 11.39 | 0.07611 | 0.511712 | 6 | 1.59 | 0.511648 | −0.61 | −16.1 | 1.59 | 101.1 | 800.0 | 0.3658 | 0.708649 | 13 | 0.7080 | This study |
| Yunfengding | AG | YFD-1 | 4.671 | 30.91 | 0.09138 | 0.511757 | 7 | 1.73 | 0.511679 | −0.54 | −15.4 | 1.73 | 84.20 | 1036 | 0.2354 | 0.708492 | 7 | 0.7081 | This study |
| | AG | YFD-5 | 5.102 | 34.46 | 0.08955 | 0.511768 | 9 | 1.69 | 0.511684 | −0.54 | −15.0 | 1.69 | 87.80 | 994.1 | 0.2557 | 0.708936 | 9 | 0.7084 | This study |
| | AG | YFD-3 | 4.562 | 32.04 | 0.08611 | 0.511705 | 6 | 1.72 | 0.511624 | −0.56 | −16.2 | 1.72 | 87.16 | 1061.1 | 0.2378 | 0.708731 | 21 | 0.7082 | This study |
| | AG | YFD-8 | 4.867 | 32.94 | 0.08937 | 0.511749 | 5 | 1.71 | 0.511665 | −0.55 | −15.4 | 1.71 | 81.91 | 1020 | 0.2325 | 0.708479 | 11 | 0.7080 | This study |
| | AG | YFD-9 | 4.111 | 30.59 | 0.08129 | 0.511724 | 11 | 1.64 | 0.511648 | −0.59 | −15.7 | 1.64 | 92.20 | 986.9 | 0.2705 | 0.709245 | 11 | 0.7087 | This study |
| | AG | Y-1 | 5.402 | 36.07 | 0.09059 | 0.511785 | 5 | 1.69 | 0.511700 | −0.54 | −14.7 | 1.69 | 83.36 | 1058 | 0.2280 | 0.708402 | 7 | 0.7079 | This study |
| Egongbao | AG | EGB-1 | 2.894 | 17.14 | 0.1021 | 0.511800 | 12 | 1.84 | 0.511705 | −0.48 | −14.6 | 1.84 | 57.45 | 649.6 | 0.2560 | 0.707992 | 9 | 0.7075 | This study |
| | AG | EGB-2 | 4.63 | 37.8 | 0.07408 | 0.511715 | 12 | 1.56 | 0.511646 | −0.62 | −15.8 | 1.56 | 120.9 | 680.8 | 0.5141 | 0.708458 | 7 | 0.7074 | This study |
| | AG | EGB-5 | 15.53 | 99.96 | 0.09398 | 0.511667 | 16 | 1.88 | 0.511580 | −0.52 | −17.1 | 1.88 | 89.98 | 1630 | 0.1598 | 0.707538 | 8 | 0.7072 | This study |
| | AG | EGB-7 | 2.692 | 16.58 | 0.0982 | 0.511610 | 8 | 2.03 | 0.511519 | −0.50 | −18.3 | 2.03 | 160.8 | 531.0 | 0.8769 | 0.709701 | 13 | 0.7079 | This study |
| | AG | EGB-8 | 2.141 | 12.3 | 0.1053 | 0.511777 | 10 | 1.92 | 0.511679 | −0.46 | −15.1 | 1.92 | 121.0 | 681.0 | 0.5144 | 0.708456 | 9 | 0.7074 | This study |
| | GD | EGB-6 | 8.266 | 53.87 | 0.0928 | 0.511558 | 10 | 2.00 | 0.511479 | −0.53 | −19.4 | 2.00 | 225.1 | 226.1 | 2.883 | 0.714558 | 8 | 0.7092 | This study |
| Baiyashan | G | BYS-2 | | | 0.1012 | 0.511520 | 7 | 2.20 | 0.511434 | −0.49 | −20.2 | 2.20 | | | 3.043 | 0.716750 | 4 | 0.7111 | Ma et al. (1998) |
| | G | B11-2 | | | 0.1058 | 0.511612 | 7 | 2.16 | 0.511522 | −0.46 | −18.5 | 2.16 | | | 5.670 | 0.723400 | 1 | 0.7129 | Ma et al. (1998) |
| Hongzhen | AG | aq-5 | 3.149 | 21.6 | 0.08870 | 0.511656 | 9 | 1.82 | 0.511586 | −0.55 | −17.5 | 1.82 | 99.14 | 453.7 | 0.6323 | 0.708207 | 17 | 0.7071 | Wang et al. (2004a) |
| | AG | aq-6 | 3.265 | 21.86 | 0.09090 | 0.511682 | 11 | 1.82 | 0.511609 | −0.54 | −17.0 | 1.82 | 97.60 | 432.6 | 0.6528 | 0.708354 | 14 | 0.7072 | Wang et al. (2004a) |
| | AG | aq-6-2 | 3.114 | 19.47 | 0.09672 | 0.511629 | 11 | 1.98 | 0.511552 | −0.51 | −18.1 | 1.98 | 100.8 | 452.2 | 0.6451 | 0.708204 | 10 | 0.7071 | Wang et al. (2004a) |

AG, adakitic granite; GD, granitic dike; G, granite.

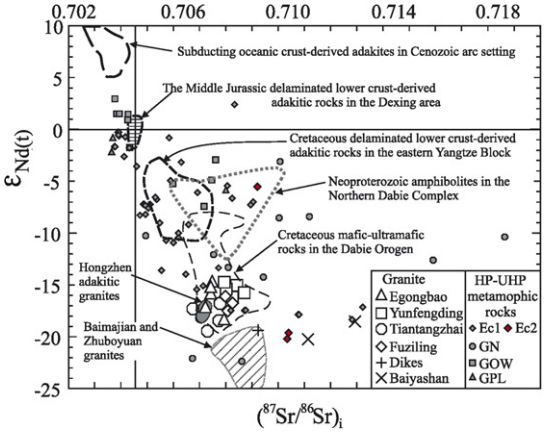


Fig. 8. Nd–Sr isotope compositions of Cretaceous adakitic granites and granitic dikes in the Northern Dabie Complex. Ec1, eclogites in or interlayers with gneisses and ultramafic rocks; Ec2, eclogites in or interlayers with marbles; GN, gneiss; GOW, garnet pyroxenite–orthopyroxenite–websterite; GPL, garnet peridotite–garnet lherzolite. Data source are as follows: the adakitic granites and granitic dikes in the Jiuzihe–Zhangjiazui area are from Table 3; Cretaceous mafic–ultramafic rocks in the Dabie Orogen are from Chen et al. (1998), Jahn et al. (1999), Li and Yang (2003), Wang and Deng (2002), and references therein; the Baiyashan, Baimajian and Zhuboyuan granites are from Ma et al. (1998), Chen et al. (2002) and Bryant et al. (2004); Cenozoic subducted oceanic crust-derived adakites are after Defant et al. (1992), Kay et al. (1993), Aguillón-Robles et al. (2001); delaminated lower crust-derived adakitic rocks are from Xu et al. (2002), Wang et al. (2004a,b, 2006a,b); the Hongzhen Cretaceous adakitic granites are from Wang et al. (2004a); Triassic HP-UHP eclogites and gneisses in the Dabie–Sulu Orogen are from Jahn (1998), Li et al. (2000), and references therein; Neoproterozoic amphibolites in the Northern Dabie Complex are from Ma et al. (2000) and Bryant et al. (2004).

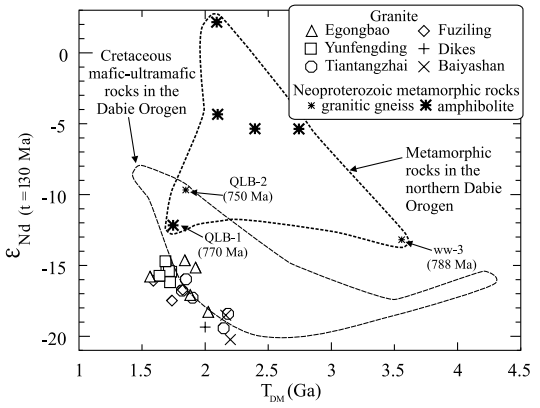


Fig. 9. Nd model age ($T_{DM}$) versus $\varepsilon_{Nd}(t = 130\ Ma)$ for the adakitic granites and granitic dikes in the Jiuzihe–Zhangjiazui area compared to amphibolites and gneisses in the Northern Dabie Complex (Ma et al., 2000; Bryant et al., 2004) and Cretaceous mafic–ultramafic rocks in the Dabie Orogen (Jahn et al., 1999; Wang and Deng, 2002, and references therein).

Moreover, discordant or concordant zircon core ages of ~1500–1700 Ma in the early Egongbao and Yunfengding adakitic granites have not been recovered from the

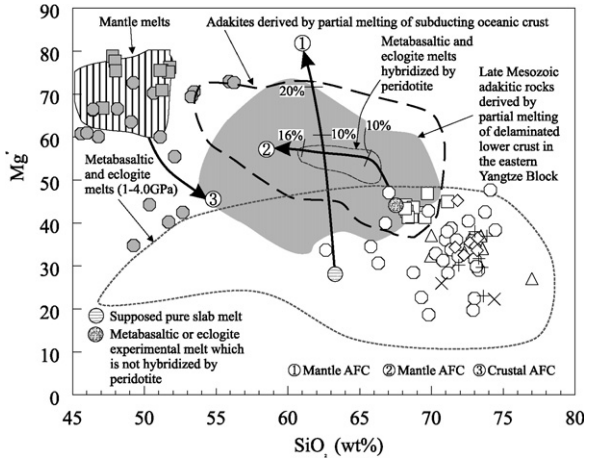


Fig. 10. $Mg^{\#}$ versus $SiO_2$ (wt%) diagrams for the adakitic granites in the Jiuzihe–Zhangjiazui area. Mantle AFC curves are after Stern and Kilian (1996) (curve 1) and Rapp et al. (1999) (curve 2), and the proportion of assimilated peridotite is also shown. The crustal AFC is after Stern and Kilian (1996) (curve 3). The jumping-off point of Curve 1 represents the composition of a pure slab melt, which is supposed by Stern and Kilian (1996). The jumping-off point of Curve 2 represents the composition of a metabasaltic or eclogite experimental melt, which is not hybridized by peridotite (Rapp et al., 1999). Fields of delaminated lower crust-derived adakitic rocks, subducted oceanic crust-derived adakites are constructed using the same data sources as in Fig. 8. Data of metabasaltic and eclogite experimental melts (1–4.0 GPa) and mafic–ultramafic intrusive rocks are from the same data sources as in Fig. 3. The field of metabasaltic and eclogite experimental melts hybridized with peridotite is after Rapp et al. (1999). Sample symbols are the same as those in Fig. 3.

700–800-Ma NDC gneisses and amphibolites, which possess no zircon ages greater than 1088 Ma (e.g., Bryant et al., 2004).

Experimental data also suggests that the adakitic granites could not be generated by the partial melting of the tonalitic orthogneisses in the Dabie Orogen (Fig. 3; Bryant et al., 2004) on the basis of the following evidence:

(1) Melting in the system tonalite–$H_2O$ generally produces tonalitic and trondhjemitic magmas (Fig. 3a) that have higher ANK ($Al_2O_3/(Na_2O + K_2O)$) values (Fig. 3c) and lower $K_2O$ contents (Fig. 4a) than the early granites. Moreover, the amount of pore fluid in the deep continental crust is likely to be small (e.g., Rutter and Wyllie, 1988), implying that natural equivalents of the experimental tonalite–$H_2O$ systems are restricted to special settings, mainly subduction zones.

(2) Dehydration melting of tonalites at pressures less than 0.8 GPa will generate A-type granites (Patiño Douce and McCarthy, 1998 and references therein) with low $Al_2O_3$ (generally $\leqslant$12 wt%) and high Y, Nb, and HREE contents and distinct negative Eu and Sr anomalies (e.g., Whalen et al., 1987), which are completely different from those of the adakitic early granites.

(3) High-pressure (1.0–3.2 GPa) dehydration melting of tonalites produces granitic melts with $SiO_2$ of more than 70 wt% and slightly to strongly peraluminous compositions (Fig. 3b and c). However, many samples of the adakitic

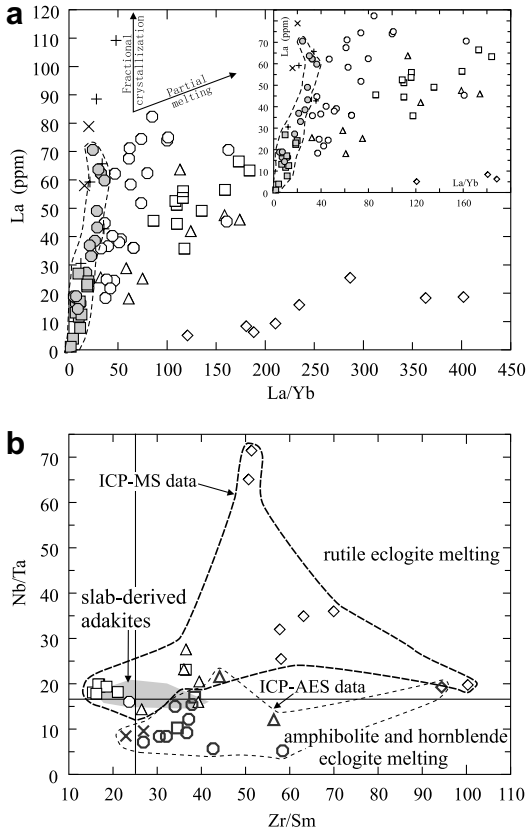


Fig. 11. (a) La/Yb versus La diagram for the adakitic granites and granitic dikes in the Jiuzihe–Zhangjiazui area and mafic–ultramafic intrusive rocks in the Dabie Orogen. (b) Nb/Ta versus Zr/Sm diagram (Condie, 2005), Lines represent primitive mantle values from Sun and McDonough (1989) and melting fields from Foley et al. (2002). The field of slab-derived adakites is after Condie (2005). The ICP-MS and ICP-AES data of the adakitic granites in the Jiuzihe–Zhangjiazui area are from the Table 2. Sample symbols are the same as those in Fig. 3.

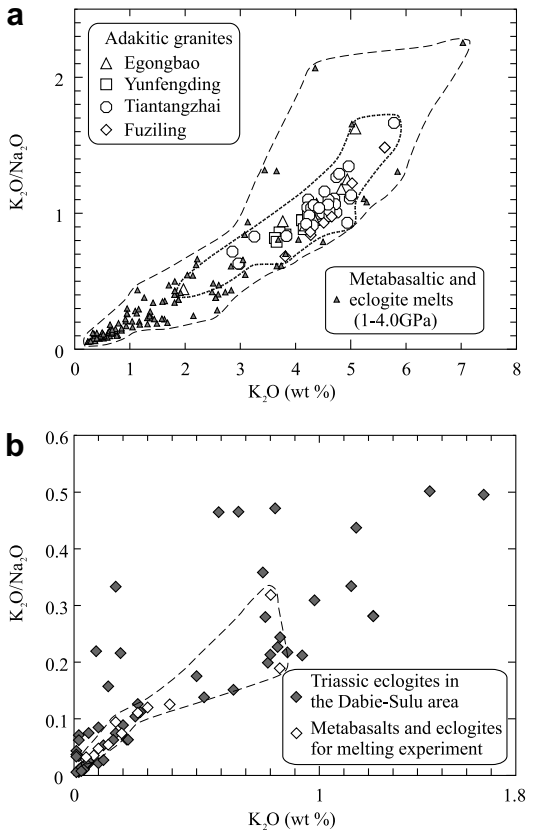


Fig. 12. $K_2O/Na_2O$ versus $K_2O$ diagrams for the Jiuzihe–Zhangjiazui adakitic granites and metabasaltic and eclogite melts (1–4.0 GPa) (a), and Triassic eclogites in the Dabie–Sulu area and Metabasalts and eclogites for melting experiment (b). The data for metabasalt and eclogite and their melts (1–4.0 GPa) are from Sen and Dunn (1994), Rapp and Watson (1995), Rapp et al. (1999, 2002, 2003), Skjerlie and Patiño Douce (2002), and references therein. The data for Triassic eclogites in the Dabie–Sulu area are from Jahn (1998), Li et al. (2000), and references therein. The data for the experimental melts with high $K_2O$ contents (3.05–7.03 wt%) and $K_2O/Na_2O$ ratios (0.66–2.25) are from Sen and Dunn (1994), Rapp et al. (1999, 2002), and Skjerlie and Patiño Douce (2002).

granites have $SiO_2$ contents ranging from 60 to 70 wt% (Fig. 3b), and all samples are metaluminous to slightly peraluminous (Fig. 3c), arguing against high-pressure dehydration melting of tonalite gneisses.

In contrast, high-pressure (1.0–4.0 GPa) dehydration melting of metabasaltic rocks and eclogites can readily generate high-K granitic melts (Figs. 3 and 4a). Experimental data suggests that $K_2O$ content of melts are mainly controlled by the $K_2O$ contents of source rocks, high pressure and dehydration melting, indicating that K-rich metabasalts/gabbros/eclogites are suitable source rocks for K-rich adakitic rocks (Sen and Dunn, 1994; Prouteau et al., 2001; Rapp et al., 2002; Skjerlie and Patiño Douce, 2002; Xiao and Clemens, 2007). For example, the alkali basaltic starting material ($K_2O = 0.82$ wt%, $K_2O/Na_2O = 0.32$) used by Sen and Dunn (1994) produced melts with $K_2O$ contents (3.05–5.85 wt%) and $K_2O/Na_2O$ ratios (0.66–1.31) comparable to the NDC adakitic rocks with $K_2O$ contents (2.94–5.74 wt%) and $K_2O/Na_2O$ ratios (0.63–1.64) at $P = 1.5$–2 GPa and $T = 900$–950 °C (Fig. 12). However, the experiments of Rapp et al. (2002, 1999), Skjerlie and Patiño Douce (2002) demonstrate that the melting of even low-K metabasaltic rocks (0.08–0.21 wt% $K_2O$ and 0.04–0.19 $K_2O/Na_2O$) can also generate adakitic magmas with appropriate $K_2O$ contents (3.53–7.03 wt%) and $K_2O/Na_2O$ ratios (0.61–2.25) at high pressure and temperature (2.7–3.8 GPa; 1000–1200 °C; Fig. 12a). Additionally, dehydration melting more readily gives rise to K-rich melts than fluid-present melting (e.g., Prouteau et al., 2001). Many Triassic eclogites in the Dabie–Sulu area exhibit higher $K_2O$ contents and $K_2O/Na_2O$ ratios than the starting materials (e.g., metabasalts and eclogite) used for melting experiments (Fig. 12b) (e.g., Sen and Dunn, 1994; Prouteau et al., 2001; Rapp et al., 2002; Skjerlie and Patiño Douce, 2002). Dehydration melting of such a source, involving the breakdown of hornblende or zoisite (e.g., Sen and Dunn, 1994; Skjerlie and Patiño Douce, 2002; Patiño Douce, 2005) at high pressures (>2 GPa) and temperature

(>900 °C), could generate the high-K adakitic rocks of the central NDC. New experimental data derived from near-whole melting of Tiantangzhai adakitic granite samples (Xiao and Clemens, 2007) further suggest that the original magma could only be generated at high temperature (>1050 °C) and pressure (>2 GPa).

The relatively high $Al_2O_3$ and Sr and very low Y and Yb contents, combined with negligible to positive Eu and Sr anomalies in the early granites are suggestive of garnet but little or no plagioclase in the source residue after melt extraction (e.g., Wilson, 1989; Defant and Drummond, 1990; Atherton and Petford, 1993). Fig. 7 illustrates that the compositions of these adakitic granites are distributed along the partial melting curves of eclogite, hornblende eclogite and garnet amphibolite. Experimental studies (e.g., Rapp et al., 2003 and references therein) have also shown that mafic crustal rocks can melt to produce adakitic liquids at sufficient depths (>40 km, i.e., ~1.2 GPa) for garnet to be stable within the residual assemblage (e.g., garnet–amphibolite, amphibole-bearing eclogite and/or eclogite). The Nd–Sr isotopic compositions of the adakitic granites of the study area are comparable to those of Cretaceous adakitic rocks of the Hongzhen area of the Eastern Yangtze Block, east of the Tanlu Fault (Fig. 1a), which Wang et al. (2004a) showed were most plausibly derived by partial melting of thickened lower crust (Fig. 8). Notably, all samples from the central NDC study area and Hongzhen adakitic rocks plot in the field of Triassic eclogites in the Dabie–Sulu Orogen in Fig. 8. Moreover, zircon core or upper intercept ages of ~1300–2000 Ma for NDC Cretaceous granitic rocks (Xue et al., 1997; Bryant et al., 2004), including the adakitic granites (Table 1), are broadly consistent with previously reported ages from an upper concordia intercept and the discordant or concordant ages of zircon cores from the UHP zone, which span 700–2347 Ma (Maruyama et al., 1998; Ayers et al., 2002; Liu et al., 2004, 2006). In summary, derivation of the NDC adakitic granites by partial melting of thickened eclogitic lower crust is consistent with both numerous experimental results and with specific chemical and isotopic data from the Dabie–Sulu Orogen.

The Nb/Ta ratios of adakitic rocks provide a means of distinguishing rutile eclogite melting from amphibolite and hornblende eclogite melting (e.g., Condie, 2005). In this study, we use only high precision ICP-MS Nb and Ta data, as suggested by Condie (2005), which indicates that Nb/Ta ratios of three of the early adakitic granites (the Egongbao, Yunfengding and Tiantangzhai granites) are close to or somewhat higher than the primitive mantle value of 16.7. In contrast, the Nb/Ta (19.8–71.4) ratios of the early Fuziling adakitic granite is distinctly higher than the primitive mantle value (Fig. 11b). High Nb/Ta ratios (>16.7) in the adakitic magmas can be attributed to one of two possible causes: (a) a source with similar high Nb/Ta ratios (Rapp et al., 2003; Xiong et al., 2005) or (b) partial melting of eclogites in the rutile stability field, given that the distribution coefficient of Ta between rutile and melt is significantly greater than that of Nb (e.g., Foley et al., 2002; Xiong et al., 2005; Xiao et al., 2006). The similar Nd–Sr isotope compositions of both the Fuziling ($129 \pm 3$ Ma) and older (131–143 Ma: Egonbao, Yunfengding, and Tiantangzhai) adakitic granites (Figs. 8 and 9) suggest that they have similar source rocks and therefore argue against a unique high Nb/Ta source for the Fuziling intrusion. As a consequence, the Egongbao, Yunfengding, and Tiantangzhai adakitic granites were probably generated on the boundary between rutile eclogite and hornblende eclogite melting whereas the slightly younger Fuziling granite was likely derived by rutile eclogite melting (Fig. 11b). The fact that the composition of the Fuziling adakitic granite samples are distributed along the partial melting curve of eclogite but other adakitic granite samples are distributed along the partial melting curves of hornblende eclogite and garnet amphibolite in Fig. 7b, further supports this distinction.

### 6.3. Petrogenesis of the late granitic dikes in the NDC

The late granitic dikes exhibit geochemical characteristics that differ from the adakitic granites in the study area (e.g., negative Eu and Sr anomalies, higher Y and Yb contents, distinct $(^{87}Sr/^{86}Sr)_i$; Figs. 6–8), suggesting that their petrogenesis differs from the larger intrusions. However, their geochemical and isotopic characteristics are similar to the late Baimajian, Zhuboyuan, and Baiyashan granites located to the east and west of the studied area (Figs. 3–8), which suggest the dikes formed by petrogenetic mechanisms similar to the latter. Zhang et al. (2002a), Chen et al. (2002), and Bryant et al. (2004), have all suggested that some or all of the late granites may have been generated by partial melting of NDC Neoproterozoic gneisses and amphibolite basement rocks, which must have had significant plagioclases in the residue to produce negative Eu and Sr anomalies of the granites (Ma et al., 1998). This model is in agreement with Gao et al. (1998a,b), who proposed that the present lower crust of the Dabie Orogen mainly consists of intermediate granulites. On this basis, we suggest that genesis of the late (118–105 Ma) granitic dikes was related to a widespread partial melting event in lower crustal granulites of the Dabie Orogen.

### 6.4. Petrogenetic implications for the Cretaceous mafic–ultramafic intrusions

A wide variety of genetic models have been proposed for the origin of Cretaceous (130–123 Ma) mafic–ultramafic intrusive rocks in the NDC and UHP–HP terrane (Fig. 1b), but until the geochronological and geochemical results of the present study there was no obvious requirement that their genesis must be consistent with the coeval formation of adakitic magmas.

We suggest that any petrogenetic model for the mafic–ultramafic intrusive rocks of the Dabie Orogen must explain the following features: (a) the suite is distributed across the whole Dabie Orogen to the south of Triassic suture between the Yangtze Block and Northern China Block (i.e., in the footwall—Yangtze Block (e.g., Hacker et al., 1998, 2000; Chen et al., 2003; Bryant et al., 2004)) and formed in an extensional setting (e.g., Ratschbacher et al.,

2000; Tsai et al., 2000); (b) zircon age data (Li et al., 1999; Wang and Deng, 2002; Zhao et al., 2005) indicates they formed at 130–123 Ma, postdating Triassic (245–210 Ma) continental subduction and the earliest adakitic granites (e.g., the 143–142 Ma Yunfengding and Egongbao granites), but contemporaneous with the 131–129 Ma Tiangtangzhai and Fuziling adakitic granites, and predating the non-adakitic 118–105 Ma Bamajian, Zhuboyuan or Baiyashan granites. (c) olivine mineral compositions (Jahn et al., 1999; Tsai et al., 2000) and ubiquitous low $FeO_T/MgO$ and high MgO or $Mg^{\#}$ and Ni values (Figs. 3b, 4d, 5a, and 10) suggest that these rocks must be derived from mantle peridotites, because partial melting of metabasaltic and eclogite only generates the mafic-felsic melts with high $FeO_T/MgO$ and low MgO or $Mg^{\#}$ values (Figs. 3b, 4d, and 10); (d) the mafic–ultramafic intrusive rocks are characterized by the high-LREE enrichment, pronounced negative Nb and Ti anomalies, and positive Ba anomalies similar to those of adakitic granites in the Jiuzihe–Zhangjiazui area, and low $\varepsilon Nd(t)$ (−8.5 to −19.5) or $(^{143}Nd/^{144}Nd)_i$ (0.5115–0.5120) combined with relatively high $(^{87}Sr/^{86}Sr)_i$ (0.7067–0.7094) (Chen et al., 1998; Ma et al., 1998; Jahn et al., 1999; Wang and Deng, 2002); (e) the Pb isotope compositions of the mafic–ultramafic intrusive rocks are close to that of the Mesozoic granitoids and eclogites from the Dabie–Sulu Orogen (Huang et al., 2007).

Petrogenesis of 143–129 Ma adakitic granites suggests that the thickened (>40–50 km) eclogitic lower crust still existed beneath the Dabie Orogen in the early Cretaceous, because the stability pressure of garnet and rutile is more than 1.2–1.5 GPa (e.g., Rapp et al., 1999; Xiong et al., 2005). The experimental data regarding approximately whole melting of the Tiantangzhai adakitic granite samples (Xiao and Clemens, 2007) further suggests that their magma could only be generated at high pressure (>2 GPa, i.e., >66 km crustal thickness). Given that eclogite has a higher density than mantle peridotite, these melting events are most plausibly linked to lower crustal delamination or foundering beneath the Dabie Orogen in the early Cretaceous (e.g., Arndt and Goldstein, 1989; Kay and Kay, 1991; Rudnick, 1995, and references therein). Geochemical and geophysical data suggest that the present lower crust of the Dabie Orogen mainly consists of intermediate granulites (e.g., Gao et al., 1998a,b) and the present thickness of crust in the Dabie area is less than ~41.5 km (e.g., Wang et al., 2000a). Lower crustal delamination or foundering can account for this thinning process (e.g., Gao et al., 1998a,b), although the crustal extension resulting from the Cretaceous doming of the NDC cannot be neglected (Ratschbacher et al., 2000). Taking into account the five key features noted above and the petrogenesis of the Cretaceous adakitic granites, we proposed a new model for the genesis of the mafic–ultramafic rocks: partial melting of a source formed by the mixing of asthenospheric mantle (Lustrino, 2005) or ancient enriched lithospheric mantle of the Yangtze Block (e.g., Wang et al., 2006b) and eclogitic lower crust mobilised by delamination or foundering. Given the similarity of the adakitic granites, mafic–ultramafic rocks, and the Dabie–Sulu UHP–HP eclogites in terms of Nd–Sr isotopic compositions and shared trace element characteristics such as positive Ba anomalies (Fig. 4 of Zhao et al., 2005 and Figs. 6 and 8), the partial melting of the mixed source could generate the mafic–ultramafic rocks. Our model is supported by the O isotopic study of zircons in Dabie–Sulu pyroxenites by Xia et al. (2002). Based on the range of isotopic compositions in the zircons and evidence that they did not undergo re-equilibration, these authors argue that mixing of mafic lower crust and mantle must have occurred in less than several million years. They also calculated that these magmas probably contained a large proportion (>37%) of mafic lower crust.

### 6.5. Geodynamic model for lower crustal melting and delamination

The prerequisite conditions for lower crustal delamination generally include (a) crustal thickening and (b) high temperature. Crustal thickening that results from shortening may result in a crustal root that, due to gabbro–eclogite phase transformation, becomes denser than the underlying mantle lithosphere (e.g., Kay and Kay, 1991, 1993). Instability times calculated for a two-dimensional Rayleigh–Taylor convective instability, where a dense lower crustal layer sinks into a lower-density mantle, show that high temperatures (>700 or >500–700 °C with a background strain rate) are required for this process to occur on a timescale of 10 Ma with rheological parameters expected for the crust and mantle (Jull and Kelemen, 2001). In the Dabie area, high temperature probably caused melting of eclogitic lower crust to generated early Cretaceous adakitic magmas, which left denser resitite minerals that strongly favoured lower crustal foundering or delamination (e.g., Arndt and Goldstein, 1989).

#### *6.5.1. Crustal thickening*

Numerous detailed studies of the Dabie Orogen HP–UHP metamorphic rocks have gradually established a consensus that UHP–HP metamorphism occurred between 245 and 210 Ma and was followed by the "rapid cooling" between 210 and 170 Ma (e.g., Hacker et al., 1998, 2000; Li et al., 2000; Ayers et al., 2002; Liu et al., 2004). These ages can be best explained by the diachronous exhumation of UHP–HP metamorphic units in response to Triassic subduction (Fig. 13a and b) (e.g., Hacker et al., 2000, 2004; Liu et al., 2004). In this model, the subduction of slices of the Yangtze continental crust was facilitated by the nearly concomitant uplift of older overlying slices during the 245–210 Ma interval (Fig. 13a). Subduction of continental fragments continued up to the Middle to Late Jurassic boundary (~159 Ma: e.g., Gilder and Courtillot, 1997; Gilder et al., 1999), but was associated with the 210–170 Ma southward thrusting of previously exhumed UHP–HP slices in the Yangtze Block (e.g., Liu et al., 2004; Fig. 13b). The combination of southward thrusting and coeval normal sense shear from beneath the Northern China Block, led to an upward extrusion of the subducted slices onto the Yangtze Block (Fig. 13b; Hacker et al., 2000, 2004; Liu et al., 2004).

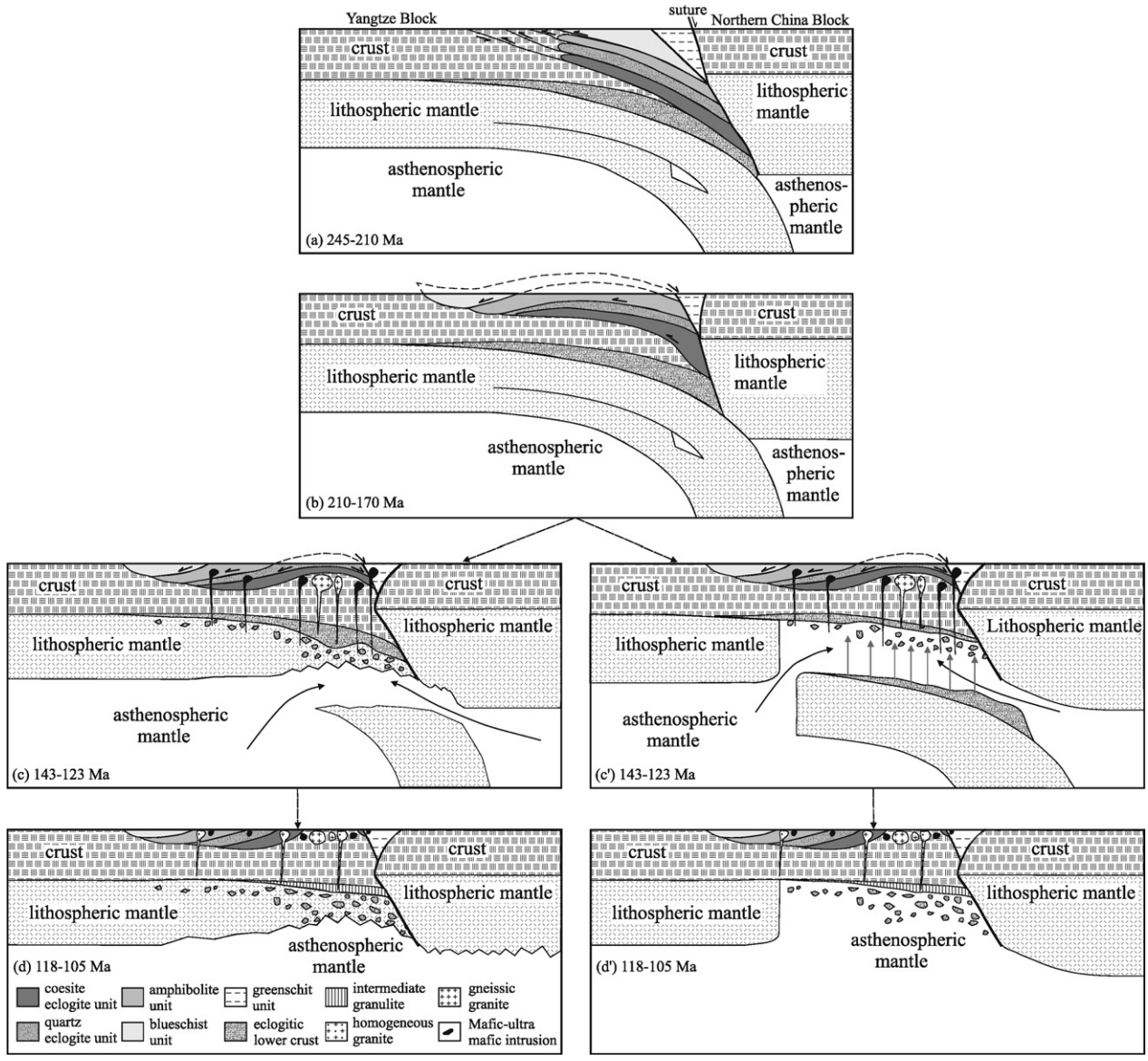


Fig. 13. A suggested model to produce the Dabie Cretaceous magmatic rocks including adakitic granites via partial melting of thickened lower crust. (a) Successive subduction of underlying slices with nearly concomitant uplift of overlying slices during the Trias1sic (240–210 Ma) collision between the Northern China Block and the Yangtze Block (modified from Hacker et al., 2000 and Liu et al. (2004)). (b) Extrusion and thrusting of subducted slices onto the Yangtze Block during the Jurassic (210–170 Ma) convergence (modified from Liu et al. (2004)). In the Stages (a) and (b), the crust and lithospheric mantle beneath the orogen were probably thickened. (c) Doming and partial melting of eclogitic lower crust and enriched upper lithospheric mantle, in response to a hot asthenosphere upwelling possibly resulting from delamination of lower lithospheric mantle during 143–123 Ma. (d) Successive upwelling of hot asthenosphere lead to partial melting of intermediate granulites during 118–105 Ma. (c′) Doming and partial melting of eclogitic lower crust and changed asthenospheric mantle, in response to an hot asthenosphere upwelling resulting from delamination of whole lithospheric mantle as well as the lower part of lower crust during 143–123 Ma. $SiO_2$-rich partial melts derived from delaminated lower crust possibly metasomatised the uprising asthenospheric mantle (thick and straight arrows) (Lustrino, 2005) and caused the formation of enriched mantle source of mafic–ultramafic rocks. (d′) Successive upwelling of hot asthenosphere lead to partial melting of intermediate granulites during 118–105 Ma. In the Stages (c and d or c′ and d′), the delamination or foundering of the eclogitic lower crust was an important geodynamic process which took place beneath the orogen.

In addition to the subduction of the Yangtze Block and exhumation of the UHP–HP metamorphic rocks, we suggest that another important process—the thickening of the crust and lithospheric mantle beneath the orogen must be taken into account. Crustal thickening would clearly occur as a result of the successive subduction or thrusting episodes (e.g., Tapponnier et al., 2001) and would produce a transformation of mafic lower crust to eclogite (e.g., Kay and Kay, 1991, 1993; Lustrino, 2005; Fig. 13a and b) as the lithosphere was simultaneously depressed to greater depths. The occurrence of the Early Cretaceous adakitic granites originating from lower crust also indicates that an eclogitic source remained in the lower crust beneath the Dabie Orogen until that time.

*6.5.2. Heat source for melting and delamination*

To date, no Triassic–Jurassic magmatic rocks have been reported in the Dabie Orogen, which argues against any early episode of crustal extension or asthenospheric upwelling. Although many researchers document large-scale Early Cretaceous igneous rocks in the area, the mechanism for generating these magmas remains contentious. Recent studies have suggested a variety of heat sources for Cretaceous magmatism in the Dabie Orogen including (a) asthenospheric upwelling in response to Pacific back-arc extension (Ratschbacher et al., 2000, 2003; Tsai et al., 2000), (b) slab breakoff (Ma et al., 1998), (c) lithospheric thinning or delamination (Chung et al., 1997; Qian et al., 2003; Bryant et al., 2004; Wu et al., 2005) or (d) a Cretaceous superplume event (Jahn et al., 1999; Zhao et al., 2005). Space considerations do not permit a detailed review of these models. We note, however, that the magmas were emplaced in a post-collisional extensional setting. The NW–SE-oriented belt of Cretaceous magmatic rocks mainly consisting of granites is linear over a distance of ~1000 km along the Qinling–Hong'an–Dabie Orogen (Fig. 1a), suggesting that their petrogenesis was likely related to late evolution (e.g., extensional collapse) of a collisional orogen belt.

Convective instability of the lower crust in continental regions may be possible if the conductively cooled upper mantle first becomes convectively unstable (Jull and Kelemen, 2001). Convective instability of the upper mantle has been proposed as a process which might account for the observation that compressional thickening precedes extensional collapse of many orogens (e.g., Molnar et al., 1998). Commonly, the combined effect of decreased effective viscosities due to horizontal shortening and entrainment of the lower crust with a convectively down-welling upper mantle may cause dense lower crust to participate in "mantle" convective down-welling (e.g., lower crustal foundering or delamination) (e.g., Kay and Kay, 1993; Jull and Kelemen, 2001). However, if only a portion of the conductive upper mantle is convectively removed due to increased viscosities at shallow levels, then the remaining thinner conductive upper mantle would have a higher temperature, potentially allowing dense lower crustal cumulates to subsequently become unstable (e.g., Jull and Kelemen, 2001).

Cretaceous mafic–ultramafic intrusions in the Dabie Orogenic Belt (Fig. 8) resemble Cenozoic potassium-rich magmatic rocks of Tibet (e.g., Turner et al., 1996) in that both exhibit low $\varepsilon_{Nd}(t)$ and high $(^{87}Sr/^{86}Sr)_i$ values and were generated from an enriched mantle source. Based on the Tibetan example (e.g., Turner et al., 1996), it is most probable that only lower lithospheric mantle was thinned or delaminated in the Dabie Orogen. Loss of the lower lithosphere would radically increase heat flow into the base of the crust and would trigger lower crustal melting or crustal foundering (or delamination) (e.g., Menzies et al., 2007). Additionally, heating also probably converted rigid, strong and highly viscous remaining lithospheric mantle into soft, weak and less viscous asthenosphere (e.g., Niu, 2005). Whether or not this conversion took place in the Dabie area in the Early Cretaceous, the viscosities of mantle beneath the eclogitic lower crust probably decreased due to heating at that time (Jull and Kelemen, 2001; Niu, 2005), which caused the eclogitic lower crust to become unstable and sink into underlying mantle (i.e., lower crustal delamination).

The delamination or foundering of the residual eclogitic crust probably caused it to sink into the underlying hotter and more plastic lithosphere (Fig. 13c) (Xu et al., 2002; Wang et al., 2006a,b) or the asthenospheric mantle (Fig. 13c′) (e.g., Arndt and Goldstein, 1989; Kay and Kay, 1991; Rudnick, 1995; Lustrino, 2005). We suggest that upwelling of hot asthenosphere caused partial melting of eclogitic lower crust and the upper enriched lithospheric mantle containing delaminated mafic lower crust to generate Early Cretaceous (143–123 Ma) adakitic and mafic–ultramafic magmas, respectively (Fig. 13c). Alternatively, the entire lithospheric mantle as well as the lower part of lower crust may have delaminated (Fig. 13c′) (e.g., Bryant et al., 2004). In this case, partial melting of the remaining intact upper part of lower crust would generate the adakitic magmas. Metasomatic reactions between $SiO_2$-rich partial melts derived from delaminated lower crust and the upwelling asthenospheric mantle (replacing the volume formerly occupied by the detached lithospheric mantle and lower part of the lower crust) lead to the formation of enriched mantle source (e.g., Arndt and Goldstein, 1989; Lustrino, 2005). Partial melting of such a source generated mafic–ultramafic magmas with low $\varepsilon_{Nd}(t)$ and relatively high $(^{87}Sr/^{86}Sr)_i$ values (Fig. 8) and Pb isotope compositions similar to Triassic eclogites (Huang et al., 2007). At the same time, the upwelling of hot asthenosphere may have initiated crustal extension and doming in the Dabie Orogen (Ratschbacher et al., 2000, 2003; Bryant et al., 2004; Hacker et al., 2004; Liu et al., 2004) (Fig. 13c and c′). Additionally, widespread Early Cretaceous plutonism in the NDC likely accelerated this extension and doming (e.g., Hollister, 1993; Hill et al., 1995). Thus, the UHP–HP metamorphic rock slices in the NDC were quickly eroded (Fig. 13c and c′).

With the continued upwelling of hot asthenosphere and the delamination of eclogitic lower crust, the intermediate granulites above the eclogitic lower crust of the Dabie Orogen were also heated and began to be melt to generate late granitic magmas between 118 and 105 Ma (Fig. 13d and d′) (e.g., Chen et al., 2002; Bryant et al., 2004). Given that the UHP–HP metamorphic rock slices in the NDC continued to be uplifted and eroded throughout this period (Fig. 13d and d′), relict UHP mafic rocks just south of the Xiaotian–Mozitang fault probably represent the portion of the slab that penetrated most deeply into the mantle and experienced the highest pressures (e.g., Bryant et al., 2004; Hacker et al., 2004).

## 7. CONCLUSIONS

(1) Early Cretaceous (143–129 Ma) adakitic granites in the Northern Dabie Complex are directly associated with a contemporary extensional structure (e.g., a metamorphic core complex) in the interior of a continent.

(2) These adakitic granites were most probably generated by partial melting of amphibole or rutile eclogites similar to Triassic eclogites in the Dabie–Sulu Orogen. The

granites most plausibly originated from lower crust that was thickened (>40–50 km) as a result of Triassic–Middle Jurassic subduction and thrusting.

(3) Dense eclogitic lower crust mixed with the underlying lithospheric or asthenospheric mantle, possibly by delamination or foundering. The early Cretaceous mafic–ultramafic intrusive rocks in the Dabie Orogen were derived from the resulting mixed or hybrid source.

(4) Late granitic dikes in the adakitic intrusions were generated by the melting of plagioclase-bearing intermediate granulites and have a petrogenesis similar to the 118–105 Ma granites in the Orogen. Given that the late granites occur both to the east (e.g., the Baimajian, Zhuboyuan granites: Fig. 1b) and to the west (e.g., Baiyashan granite) of the study area, the presence of the dikes demonstrate regional continuity of the late granite-forming event.

(5) The upwelling of asthenosphere, most probably in response to post-collisional delamination of lithosphere mantle, provided the heat source for the Cretaceous magmatism.

## ACKNOWLEDGMENTS

We sincerely thank associate editor Professor Martin Menzies, Drs. Sun Min, and Hugh Smithies, and two anonymous reviewers for their constructive and helpful reviews. Professors Wang Renjing, Qiu Jiaxiang, Sang Longkang and Liu Dunyi, and Tao Hua, Zhang Yuhai, Hu Zhengxiang, Dai Shengqian, He Yong, Wang Jianxin, Qi Xianmao, Zhang Shunjin, Zhu Ning, Zhang Zeming, Zhang Baomin, Xie Defan, Liu Ying, Hu Guangqian, and Chen Zhenyu are thanked for their assistance with laboratory and field work. Financial support for this research was provided by the National Natural Science Foundation of China (Grant Nos. 40421303, 40572042, and 40673037).

## REFERENCES

Aguillón-Robles A., Caimus T., Bellon H., Maury R. C., Cotton J., Bourgois J., and Michaud F. (2001) Late Miocene adakite and Nb-enriched basalts from Vizcaino Peninsula, Mexico: indicators of East Pacific Rise subduction below southern Baja California. *Geology* **29**, 531–534.

Arculus R. J., Lapierrre H., and Jaillard E. (1999) Geochemical window into subduction and accretion processes: Raspas metamorphic complex, Ecuador. *Geology* **27**, 547–550.

Arculus R. J. (2003) Use and abuse of the terms calcalkaline and calcalkalic. *J. Petrol.* **44**, 929–935.

Arndt N. T., and Goldstein S. L. (1989) An open boundary between lower continental crust and mantle: its role in crust. *Tectonophysics* **161**, 201–212.

Atherton M. P., and Petford N. (1993) Generation of sodium-rich magmas from newly underplated basaltic crust. *Nature* **362**, 144–146.

Ayers J. C., Dunkle S., Gao S., and Miller C. F. (2002) Constraints on timing of peak and retrograde metamorphism in the Dabie Shan ultrahigh-pressure belt, east-central China, using U–Th–Pb dating of zircon and monazite. *Chem. Geol.* **186**, 315–331.

Bryant D. L., Ayers J. C., Gao S., Miller C. F., and Zhang H. (2004) Geochemical, age, and isotopic constraints on the location of the Sino-Korean/Yangtze Suture and evolution of the Northern Dabie Complex, east central China. *Geol. Soc. Am. Bull.* **116**, 698–717.

Carroll M. R., and Wyllie P. J. (1989) Experimental phase relations in the system tonalite–peridotite–$H_2O$: implications for assimilation and differentiation processes near the crust–mantle boundary. *J. Petrol.* **30**, 1351–1382.

Carroll M. R., and Wyllie P. J. (1990) The system tonalite–$H_2O$ at 15 kbar and the genesis of calc-alkaline magmas. *Amer. Miner.* **75**, 345–357.

Castillo P. R., Janney P. E., and Solidum R. U. (1999) Petrology and geochemistry of Camiguin island, southern Philippines: insights to the source of adakites and other lavas in a complex arc setting. *Contrib. Mineral. Petrol.* **134**, 33–51.

Castillo P. R. (2006) An overview of adakite petrogenesis. *Chinese Sci. Bull.* **51**, 257–268.

Chen J. F., and Jahn B. M. (1998) Crustal evolution of Southeast China: Nd and Sr isotopic evidence. *Tectonophysics* **284**, 101–133.

Chen B., Jahn B. M., and Wei C. (2002) Petrogenesis of Mesozoic granitoids in the Dabie UHP complex, Central China: trace element and Nd–Sr isotope evidence. *Lithos* **60**, 67–88.

Chen D., Wu Y., Wang Y., Zhi X., Xia Q., and Yang J. (1998) Ages, Nd and Sr isotopic compositions of the Jiaoziyan gabbroic intrusion from the northern Dabie terrain. *Sci. Geol. Sin.* **7**, 29–35.

Chen F., Guo J., Jiang L., Siebel W., Cong B., and Satir M. (2003) Provenance of the Beihuaiyang lower-grade metamorphic zone of the Dabie ultrahigh-pressure collisional orogen, China: evidence from zircon ages. *J. Asian Earth Sci.* **120**, 131–148.

Chung S. L., Lo C. H., Li X. H., Griffin W. L., O'Reilly S. Y., and Chen C. H. (1997) From mountains to basin: a Tibetan model for the post-collisional magmatic and tectonic evolution in North China. *EOS Trans. Am. Geophys. Union* **78**, F649.

Chung S. L., Liu D. Y., Ji J. Q., Chu M. F., Lee H. Y., Wen D. J., Lo C. H., Lee T. Y., Qian Q., and Zhang Q. (2003) Adakites from continental collision zones: melting of thickened lower crust beneath southern Tibet. *Geology* **31**, 1021–1024.

Condie K. C. (2005) TTGs and adakites: are they both slab melts? *Lithos* **80**, 33–44.

Defant M. J., and Drummond M. S. (1990) Derivation of some modern arc magmas by melting of young subducted lithosphere. *Nature* **347**, 662–665.

Defant M. J., Jackson T. E., Drummond M. S., De Boer J. Z., Bellon H., Feigenson M. D., Maury R. C., and Stewart R. H. (1992) The geochemistry of young volcanism throughout western Panama and southeastern Costa Rica: an overview. *J. Geol. Soc. London* **149**, 569–579.

Defant M. J., Xu J. F., Kepezhinskas P., Wang Q., Zhang Q., and Xiao L. (2002) Adakites: some variations on a theme. *Acta Petrol. Sin.* **18**, 129–142.

Drummond M. S., and Defant M. J. (1990) A model for trondhjenite–tonalite–dactite genesis and crustal growth via slab melting: Archean to modern composition. *J. Geophys. Res.* **95**, 21503–21521.

Fan W. M., Guo F., Wang Y. J., and Zhang M. (2004) Late Mesozoic volcanism in the northern Huaiyang tectono-magmatic belt, central China: partial melts from a lithospheric mantle with subducted continental crust relicts beneath the Dabie orogen? *Chem. Geol.* **209**, 27–48.

Foley S. F., Tiepolo M., and Vannucci R. (2002) Growth of early continental crust controlled by melting of amphibolite in subduction zones. *Nature* **417**, 837–840.

Gao S., Zhang B., Gu X., Xie X., Gao C., and Guo X. (1995) Silurian–Devonian provenance changes of South Qinling Basin: implications for accretion of the Yangtze (South China) to the North China Craton. *Tectonophysics* **250**, 183–197.

Gao S., Luo T. C., and Zhang B. R. (1998a) Chemical composition of the continental crust as revealed by studies in East China. *Geochim. Cosmochim. Acta* **62**, 1959–1975.

Gao S., Zhang B. R., Jin Z. M., Kern H., Zhao Z. D., and Luo T. C. (1998b) How mafic is the lower continental crust? *Earth Planet Sci. Lett.* **161**, 101–117.

Gao S., Rudnick R. L., Yuan H. L., Liu X. M., Liu Y. S., Xu W. L., Lin W. L., Ayers J., Wang X. C., and Wang Q. H. (2004) Recycling lower continental crust in the North China craton. *Nature* **432**, 892–897.

Gilder S. A., and Courtillot V. (1997) Timing of the North–South China collision from new middle to late Mesozoic paleomagnetic data from the North China Block. *J. Geophys. Res.* **102**, 17713–17727.

Gilder S. A., Leloup P. H., Courtillot V., Chen Y., Coe R. S., Zhao X., Xiao W., Halim N., Cogné J. P., and Zhu R. (1999) Tectonic evolution of the Tancheng–Lujiang (Tan–Lu) fault via Middle Triassic to Early Cenozoic paleomagnetic data. *J. Geophys. Res.* **104**, 15365–15390.

Gromet L. P., and Silver L. (1987) REE variations across the peninsular ranges batholith: implications for batholithic petrogenesis and crustal growth in magmatic arcs. *J. Petrol.* **28**, 75–125.

Gutscher M. A., Maury R., Eissen J., and Bourdon E. (2000) Can slab melting be caused by flat subduction? *Geology* **28**, 535–538.

Hacker, B. R., Wang, X., and Eide, E. A. (1996) The Qinling–Dabie ultra-high-pressure collisional orogen. In *The Tectonics of Asia* (eds. A. Yin and T. M. Harriso). Cambridge University Press, Cambridge, pp. 345–370.

Hacker B. R., Ratschbacher L., Webb L. E., Ireland T. R., Walker D., and Dong S. (1998) U/Pb zircon ages constrain the architecture of the ultrahigh-pressure Qinling–Dabie orogen, China. *Earth Planetary Sci. Lett.* **161**, 215–230.

Hacker B. R., Ratshbacher L., Webb L. E., Ireland T. R., Calvert A., Dong S., Wenk H. R., and Chateigner D. (2000) Exhumation of ultrahigh-pressure continental crust in east-central China: Late Triassic–Early Jurassic tectonic unroofing. *J. Geophys. Res.* **105**, 13339–13364.

Hacker, B. R., Ratschbacher, L., and Liu, J. G. (2004) Subduction, collision and exhumation in the ultrahigh-pressure Qinling–Dabie orogen. In *Aspects of the Tectonic Evolution of China*, vol. 226 (eds. J. Malpas, C. Fletcher, and J. R. Ali). Geological Society, Special publication, London, pp. 157–175.

Harris N. R., Sisson V. B., Wright J. E., and Pavlis T. L. (1996) Evicence for Eocene mafic underplating, during fore-arc intrusive activity, eastern Chugach Mountains, Alaska. *Geology* **24**, 263–264.

Hermann J., Rubatto D., Korsakov A., and Shatsky V. S. (2001) Multiple zircon growth during fast exhumation of diamondiferous, deeply subducted continental crust (Kokchetav Massif, Kazakhstan). *Contrib. Mineral. Petrol.* **141**, 66–82.

Hill E. J., Baldwin S. L., and Lister G. S. (1995) Magmatism as an essential driving force for formation of active metamorphic core complexes in eastern Papua New Guinea. *J. Geophys. Res.* **100**, 10441–10452.

Hollister L. S. (1993) The role of melt in the uplift and exhumation of orogenic belts. *Chem. Geol.* **108**, 31–48.

Hou Z. Q., Gao Y. F., Qu X. M., Rui Z. Y., and Mo X. X. (2004) Origin of adakitic intrusives generated during mid-Miocene east–west extension in southern Tibet. *Earth Planet. Sci. Lett.* **220**, 139–155.

Huang F., Li S. G., Dong F., Li Q. L., Chen F. K., Wang Y., and Yang W. (2007) Recycling of deeply subducted continental crust in the Dabie Mountains, central China. *Lithos*, in press, doi:10.1016/j.lithos.2006.09.019.

Jahn, B. M. (1998) Geochemical and isotopic characteristics of UHP eclogites and ultramafic rocks of the Dabie orogen: implications for continental subduction and collisional tectonics. In *When Continents Collide: Geodynamics and Geochemistry of Ultrahigh-pressure Rocks* (eds. B. R. Hacker and J. G. Liou). Kluwer Academic Publishers, Dordrecht, pp. 203–239.

Jahn B. M., Wu F. Y., Lo C. H., and Tsai C. H. (1999) Crustal–mantle interaction induced by deep subduction of the continental crust: geochemical and Sr–Nd isotopic evidence from post-collisional mafic–ultramafic intrusions of the northern Dabie Complex, central China. *Chem. Geol.* **157**, 119–146.

Jian P., Liu D. Y., and Sun X. M. (2003) SHRIMP dating of Carboniferous Jinshajiang ophiolite in western Yunnan and Sichuan: geochronological constraints on the evolution of the Paleo-Tethys oceanic crust. *Acta Geol. Sin.* **77**, 217–277 (in Chinese with English abstract).

Jull M., and Kelemen P. B. (2001) On the conditions for lower crustal convective instability. *J. Geophys. Res.* **106**, 6423–6446.

Kay R. W., and Kay S. M. (1991) Creation and destruction of lower continental crust. *Geol. Rundsch.* **80**, 259–278.

Kay R. W., and Kay S. M. (1993) Delamination and delamination magmatism. *Tectonophysics* **219**, 177–189.

Kay R. W., and Kay S. M. (2002) Andean adakites: three ways to make them. *Acta Petrol. Sin.* **18**, 303–311.

Kay S. M., Ramos V. A., and Marquez M. (1993) Evidence in Cerro Pampa volcanic rocks of slab melting prior to ridge trench collision in southern South America. *J. Geol.* **101**, 703–714.

Kay S. M., Godoy E., and Kurtz A. (2005) Episodic arc migration, crustal thickening, subduction erosion, and magmatism in the south-central Andes. *Geol. Soc. Am. Bull.* **117**, 67–88.

Li S., and Wang T. (1991) *Geochemistry of Granitoids in the Tongbaishan–Dabieshan, Central China*. China University of Geosciences Press, Wuhan, pp. 1–208 (in Chinese with English abstract).

Li S. G., Jian H., Li H. M., and Jiang L. L. (1999) U–Pb zircon ages of the pyroxenite-gabbro intrusions in Dabie Mountains and their geological implications. *Geol. J. China Univ.* **5**, 351–355 (in Chinese, with English abstract).

Li S. G., Jagoutz E., Chen Y. Z., and Li Q. L. (2000) Sm–Nd and Rb– Sr isotopic chronology and cooling history of ultrahigh pressure metamorphic rocks and their country rocks at Shuanghe in the Dabie Mountains, Central China. *Geochim. Cosmochim. Acta* **64**, 1077–1093.

Li S. G., and Yang W. (2003) Decoupling of surface and subsurface sutures in the Dabie Orogen and a continent-collisional lithospheric wedging model: Sr–Nd–Pb isotopic evidences of Mesozoic igneous rocks in eastern China. *Chinese Sci. Bull.* **48**, 831–838.

Li X. H., Li Z. X., Zhou H. W., Liu Y., and Kinny P. D. (2002) U–Pb zircon geochronology, geochemistry and Nd isotopic study of Neoprozoic bimodal volcanic rocks in the Kangdian Rift of south China: implications for the initial rifting of Rodinia. *Precambrian Res.* **113**, 135–154.

Li X. H. (2000) Cretaceous magmatism and lithospheric extension in Southeast China. *J. Asian Earth Sci.* **18**, 293–305.

Liou, J. G., Zhang, R. -Y., Eide, E. A., Wang, X. M., Ernst, W. G., and Maruyama, S. (1996) Metamorphism and tectonics of highpressure and ultra-high-pressure belts in the Dabie–Sulu region, China. In *The Tectonics of Asia* (eds. M. T. Harrison and A. Yin). Cambridge University Press, Cambridge, pp. 300–344.

Liu D. Y., Jian P., Kröner A., and Xu S. T. (2006) Dating of prograde metamorphic events deciphered from episodic zircon growth in rocks of the Dabie–Sulu UHP complex, China. *Earth Planet. Sci. Lett.* **250**, 650–666.

Liu X. C., Jahn B. M., Liu D. Y., Dong S. W., and Li S. Z. (2004) SHRIMP U–Pb zircon dating of a metagabbro and eclogites from western Dabieshan (Hong'an Block), China, and its tectonic implications. *Tectonophysics* **394**, 171–192.

Liu Y. C., Li S. G., Xu S. T., Jahn B. M., Zheng Y. F., Zhang Z. Q., Jiang L. L., Chen G. B., and Wu W. P. (2005) Geochemistry and geochronology of eclogites from the North Dabie Mountains, central China. *J. Asian Earth Sci.* **25**, 431–443.

Ludwig K. R. (2001) Squid 1.02: A user manual. *Berkeley Geochronol. Center Special Pub.* **2**, 19.

Lustrino M. (2005) How the delamination and detachment of lower crust can influence basaltic magmatism. *Earth Sci. Rev.* **72**, 21–38.

Ma C. Q., Li Z., Ehlers C., Yang K., and Wang R. (1998) A postcollisional magmatic plumbing system: Mesozoic granitoid plutons from the Dabieshan high-pressure and ultrahigh pressure metamorphic zone, east-central China. *Lithos* **45**, 431–456.

Ma C. Q., Ehlers C., Xu C., Li Z. C., and Yang K. G. (2000) The roots of the Dabieshan ultrahigh-pressure metamorphic terrane: constraints from geochemistry and Nd–Sr isotope systematics. *Precambrian Res.* **102**, 279–301.

Maruyama S., Tabata H., Nutman A. P., Morikawa T., and Liou J. G. (1998) SHRIMP U–Pb geochronology of ultrahigh-pressure metamorphic rocks of the Dabie Mountains, central China. *Continental Dyn.* **3**, 72–85.

Martin H., Smithies R. H., Rapp R., Moyen J. F., and Champion D. (2005) An overview of adakite, tonalite–trondhjemite–granodiorite (TTG), and sanukitoid: relationships and some implications for crustal evolution. *Lithos* **79**, 1–24.

Menzies M., Xu Y. G., Zhang H. F., and Fan W. M. (2007) Integration of geology, geophysics and geochemistry: a key to understanding the North China Craton. *Lithos*, in press, doi:10.1016/j.lithos.2006.09.008.

Molnar P., Houseman G. A., and Conrad C. (1998) Rayleigh–Taylor instability and convective thinning of mechanically thickened lithosphere: effects of nonlinear viscosity decreasing exponentially with depth and of horizontal shortening of the layer. *Geophys. J. Int.* **133**, 568–584.

Niu Y. (2005) Generation and evolution of basaltic magmas: some basic concepts and a new view on the origin of Mesozoic–Cenozoic basaltic volcanism in eastern China. *Geol. J. China Univ.* **11**, 9–46.

Patiño Douce, A.E., and McCarthy, T.C. (1998) Melting of crustal rocks during continental collision and subduction. In *When Continents Collide: Geodynamics and Geochemistry of Ultrahigh-Pressure Rocks* (eds. B. R. Hacker and J. G. Liou), Kluwer Academic, Dordrecht, pp. 27–55.

Patiño Douce A. E. (2005) Vapor-absent melting of tonalite at 15–32 kbar. *J. Petrol.* **46**, 275–290.

Petford N., and Atherton M. (1996) Na-rich partial melts from newly underplated basaltic crust: the Cordillera Blanca Batholith, Peru. *J. Petrol.* **37**, 1491–1521.

Prouteau G., Scaillet B., Pichavant M., and Maury R. (2001) Evidence for mantle metasomatism by hydrous silicic melts derived from subducted oceanic crust. *Nature* **410**, 197–200.

Qian Q., Chu M. F., Chung S. L., Lee T. Y., and Xiong X. M. (2003) Was Triassic continental subduction solely responsible for the generation of Mesozoic mafic magmas and mantle source enrichment in the Dabie–Sulu orogen? *Int. Geol. Rev.* **45**, 659–670.

Qu X. M., Hou Z. Q., and Li Y. G. (2004) Melt components derived from a subducted slab in late orogenic ore-bearing porphyries in the Gangdese copper belt, southern Tibetan plateau. *Lithos* **74**, 131–148.

Rapp R. P., and Watson E. B. (1995) Dehydration melting of metabasalt at 8–32 kbar: implications for continental growth and crust–mantle recycing. *J. Petrol.* **36**, 891–931.

Rapp R. P., Shimizu N., Norman M. D., and Applegate G. S. (1999) Reaction between slab-derived melts and peridotite in the mantle wedge: experimental constraints at 3.8 Gpa. *Chem. Geol.* **160**, 335–356.

Rapp R. P., Xiao L., and Shimizu N. (2002) Experimental constraints on the origin of potassium-rich adakite in east China. *Acta Petrol. Sin.* **18**, 293–311.

Rapp R. P., Shimizu N., and Norman M. D. (2003) Growth of early continental crust by partial melting of eclogite. *Nature* **425**, 605–609.

Ratschbacher L., Hacker B. R., Webb L. E., McWilliams M., Ireland T., Dong S. W., Calvert A., Chateigner D., and Wenk H. R. (2000) Exhumation of the ultrahigh-pressure continental crust in east central China: Cretaceous and Cenozoic unroofing and the Tan–Lu fault. *J. Geophys. Res.* **105**, 13303–13338.

Ratschbacher L., Hacker B. R., Calvert A., Webb L. E., Grimmer J. C., Mcwilliams M. O., Ireland T., Dong S., and Hu J. (2003) Tectonics of the Qinling (Central China): tectonostratigraphy, geochronology, and deformation history. *Tectonophysics* **366**, 1–53.

Rowley D. B., Xue F., Tucker R. D., Peng Z. X., Baker J., and Davis A. (1997) Ages of ultrahigh pressure metamorphism and protolith orthogneisses from the central Dabie Shan: U/Pb zircon geochronology. *Earth Planet. Sci. Lett.* **151**, 191–203.

Rudnick R. L. (1995) Making continental continental crust. *Nature* **378**, 571–578.

Rutter M. J., and Wyllie P. J. (1988) Melting of vapour-absent tonalite at 10 kbar to simulate dehydration–melting in the deep crust. *Nature* **331**, 159–160.

Sen C., and Dunn T. (1994) Dehydration melting of a basaltic composition amphibolite at 1.5 and 2.0 Gpa: implications for the origin of adakites. *Contrib. Mineral. Petrol.* **117**, 394–409.

Skjerlie K. P., and Johnston A. D. (1993) Fluid-absent melting behavior of an F-rich tonalitic gneiss at mid-crustal pressures: implications for the generation of anorogenic granites. *J. Petrol.* **34**, 785–815.

Skjerlie K. P., and Patiño Douce A. E. (2002) The Fluid-absent partial melting of a zoisite-bearing quartz eclogite from 1.0 to 3.2 GPa: implications for melting in thickened continental crust and for subduction-zone processes. *J. Petrol.* **43**, 291–314.

Smithies R. H., and Champion D. C. (2000) The Archean high-Mg diorite suite: links to tonalite–trondhjemite–granodiorite magmatism and implications for early Archean crustal growth. *J. Petrol.* **41**, 1653–1671.

Steiger R. H., and Jager E. (1977) Subcommission on geochronology: convention on the use of decay constants in geo- and cosmochronology. *Earth Planet. Sci. Lett.* **36**, 359–362.

Stern C. R., and Kilian R. (1996) Role of the subducted slab, mantle wedge and continental crust in the generation of adakites from the Austral Volcanic Zone. *Contrib. Mineral. Petrol.* **123**, 263–281.

Sun, S. S., and McDonough, W. F. (1989) Chemical and isotopic systematics of oceanic basalts: implications for mantle composition and processes. In *Implications for Mantle Composition and Processes, Magmatism in the Ocean Basins*, vol. 42 (eds. A. D. Saunders and M. J. Norry). Geological Society, London, Special publication, pp. 313–345.

Sun W. D., Williams S., and Li S. G. (2002) Carboniferous and Triassic eclogites in the western Dabie Mountains, east-central China: evidence for protracted convergence of the North and South China Blocks. *J. Metamorp. Geol.* **20**, 873–886.

Suo S. T., Zhong Z. Q., Zhou H. W., and You Z. D. (2003) Massive eclogites and their tectonic significance in Dabie–Sulu ultra-high-pressure metamorphic belt, East-Central China. *Earth Sci.* **28**, 111–120 (in Chinese with English abstract).

Tapponnier P., Xu Z. Q., Roger F., Meyer B., Arnaud N., Wittlinger G., and Yang J. S. (2001) Oblique stepwise rise and growth of the Tibet plateau. *Science* **294**, 1671–1677.

Topuz G., Altherr R., Schwarz W. H., Siebel W., Satır M., and Dokuz A. (2005) Post-collisional plutonism with adakite-like signatures: the Eocene Saraycık granodiorite (Eastern Pontides, Turkey). *Contrib. Mineral. Petrol.* **150**, 441–455.

Tsai C. H., Lo C. H., Liou J. G., and Jahn B. M. (2000) Evidence against subduction-related magmatism for the Jiaoziyan Gabbro, northern Dabie Shan, China. *Geology* **28**, 943–946.

Turner S., Arnaud N., Liu J., Rogers N., Hawkesworth C., Harris N., Kelley S., van Calsteren P., and Deng W. (1996) Postcollision, shoshonitic volcanism on the Tibetan plateau: implications for convective thinning of the lithosphere and the source of ocean island basalts. *J. Petrol.* **37**, 45–71.

Wan Y. S., Li R. W., Wilde S. A., Liu D. Y., Chen Z. Y., Yan L., Song T. R., and Yin X. Y. (2005) UHP metamorphism and exhumation of the Dabie Orogen, China: evidence from SHRIMP dating of zircon and monazite from a UHP granitic gneiss cobble from the Hefei Basin. *Geochim. Cosmochim. Acta* **69**, 4333–4348.

Wang R. J., Wang Q., and He Y. (1998) The petrogenesis and age of the Jiuzihe–Tiantangzhai granites in the core of the Dabie Orogen. *Bull. Mineral. Petrol. Geochem.* **17**, 224–228 (in Chinese with English abstract).

Wang C. Y., Zeng Y. S., Mooney W. D., and Hacker B. R. (2000a) A crustal model of the ultrahigh-pressure Dabie Shan orogenic belt, China, derived from deep seismic refraction profiling. *J. Geophys. Res.* **105**, 10857–10869.

Wang J. H., and Deng S. X. (2002) Emplacement age for the mafic–ultramafic plutons in the northern Dabie Mts. (Hubei): Zircon U–Pb, Sm-Nd and $^{40}Ar/^{39}Ar$ dating. *Sci. China, Ser. D* **45**, 1–12.

Wang Q., Zhao Z., and Xiong X. (2000b) The ascertainment of Late-Yanshanian A-type granite in Tongbai–Dabie Orogenic Belt. *Acta Petrol. Mineral.* **19**, 297–306 (in Chinese with English abstract).

Wang Q., Xu J. F., Zhao Z. H., Wang R. J., Qiu J. X., and Bao Z. W. (2001) The petrogenesis and geodynamic significances of heavy rare earth element (HREE)-depleted granitoids during Yanshanian period in the Dabie Mountains. *Acta Petrol. Sin.* **17**(4), 551–564 (in Chinese with English abstract).

Wang Q., Xu J. F., Zhao Z. H., Bao Z. W., Xu W., and Xiong X. L. (2004a) Cretaceous high-potassium intrusive rocks in the Yueshan–Hongzhen area of east China: adakites in an extensional tectonic regime within a continent. *Geochem. J.* **38**, 417–434.

Wang Q., Zhao Z. H., Bao Z. W., Xu J. F., Liu W., Li C. F., Bai Z. H., and Xiong X. L. (2004b) Geochemistry and petrogenesis of the Tongshankou and Yinzu adakitic intrusive rocks and the associated porphyry copper–molybdenum mineralization in southeast Hubei, east China. *Resour. Geol.* **54**, 137–152.

Wang Q., McDermott F., Xu J. F., Bellon H., and Zhu Y. T. (2005a) Cenozoic K-rich adakitic volcanic rocks in the Hohxil area, northern Tibet: lower crustal melting in an intracontinental setting. *Geology* **33**, 465–468.

Wang Q., Zhao Z. H., Jian P., Dai T. M., Xiong X. L., Xu J. F., Bao Z. W., and Ma J. L. (2005b) Geochronology of Cretaceous A-type granitoids or alkaline intrusive rocks in the hinterland, South China: constraints for late-Mesozoic tectonic evolution. *Acta Petrol. Sin.* **21**, 795–808 (in Chinese with English abstract).

Wang Q., Xu J. F., Jian P., Bao Z. W., Zhao Z. H., Li C. F., Xiong X. L., and Ma J. L. (2006a) Petrogenesis of adakitic porphyries in an extensional tectonic setting, Dexing, South China: implications for the genesis of porphyry copper mineralization. *J. Petrol.* **47**, 119–144.

Wang Q., Wyman D. A., Xu J. F., Zhao Z. H., Jian P., Xiong X. L., Bao Z. W., Li C. F., and Bai Z. H. (2006b) Petrogenesis of Cretaceous adakitic and shoshonitic igneous rocks in the Luzong area, Anhui Province (eastern China): implications for geodynamics and Cu–Au mineralization. *Lithos* **89**, 424–446.

Whalen J. B., Currie K. L., and Chappell B. W. (1987) A-type granites: geochemical characteristics, discrimination and petrogenesis. *Contrib. Mineral. Petrol.* **95**, 407–419.

Wilson M. (1989) *Igneous petrogenesis*. Unwin Hyman, London, pp. 1–466.

Wu F. Y., Lin J. Q., Wilde S. A., Zhang X. O., and Yang J. H. (2005) Nature and significance of the Early Cretaceous giant igneous event in eastern China. *Earth Planet. Sci. Lett.* **233**, 103–119.

Xia Q. K., Deloule E., Wu Y. B., Chen D. G., and Cheng H. (2002) Oxygen isotopic compositions of zircons from pyroxenite of Daoshichong, Dabieshan: implications for crust–mantle interaction. *Chinese Sci. Bull.* **47**, 1466–1469.

Xiao L., and Clemens J. D. (2007) Origin of potassic (C-type) adakite magmas: experimental and field constraints. *Lithos*, in press, doi:10.1016/j.lithos.2006.09.002.

Xiao Y., Sun W., Hoefs J., Simon K., Zhang Z., Li S., and Hofmann A. W. (2006) Making continental crust through slab melting: constraints from niobium–tantalum fractionation in UHP metamorphic rutile. *Geochim. Cosmochim. Acta* **70**, 4770–4782.

Xie Z., Zheng Y. F., Yan J., and Qian H. (2004) Source evolution relationship between A-type granites and mafic rocks from Shacun in Dabiesha. *Acta Petrol. Sin.* **20**, 1175–1184 (in Chinese with English abstract).

Xiong X. L., Adam T. J., and Green T. H. (2005) Rutile stability and rutile/melt HFSE partitioning during partial melting of hydrous basalt: implications for TTG genesis. *Chem. Geol.* **210**, 339–359.

Xu J. F., Shinjio R., Defant M. J., Wang Q., and Rapp R. P. (2002) Origin of Mesozoic adakitic intrusive rocks in the Ningzhen area of east China: partial melting of delaminated lower continental crust? *Geology* **30**, 1111–1114.

Xu S. T., Liu Y., Chen G., Roberto C., France R., He M., and Liu H. (2003) New finding of micro-diamonds in eclogites from Dabie–Sulu region in central-eastern China. *Chinese Sci. Bull.* **48**, 988–994.

Xue F., Rowley D. B., Tucker R. D., and Peng Z. (1997) U–Pb zircon ages of granitoid rocks in the north Dabie Complex, eastern Dabie Shan, China. *J. Geol.* **105**, 744–753.

Ye K., Cong B. L., and Ye D. (2000) The possible subduction of continental material to depths greater than 200 km. *Nature* **407**, 734–736.

Zhai M., and Cong B. (1996) Petrotectonics of Sulu–Dabie metamorphic belt, central and east China. *Sci. China, Ser. D* **39**, 319–328.

Zhang Q., Qian Q., Wang E. C., Wang Y., Zhao T. P., Hao J., and Guo G. J. (2001) Existence of the East China Plateau in the mid-late Yanshan period: implications from adakites. *Sci. Geol. Sin.* **36**, 248–255 (in Chinese with English abstract).

Zhang H. F., Gao S., Zhong Z. Q., Zhang B. R., Zhang L., and Hu S. H. (2002a) Geochemical and Sr–Nd–Pb isotopic compositions of Cretaceous granitoids: constraints on tectonic framework and crustal structure of the Dabieshan ultrahigh pressure metamorphic belt China. *Chem. Geol.* **186**, 281–299.

Zhang H. F., Sun M., and Zhou X. H. (2002b) Mesozoic lithosphere destruction beneath the North China Craton: Evidence from major- and trace- elements and Sr–Nd–Pb isotope studies of Fangcheng basalts. *Contrib. Mineral. Petrol.* **144**, 241–253.

Zhang R. Y., Liou J. G., and Tsai C. H. (1996) Petrogenesis of a high temperature metamorphic terrane: a new tectonic inter-

pretation for the North Dabieshan, central China. *J. Metamorp. Geol.* **14**, 319–333.

Zhao Z. F., Zheng Y. F., Wei C. S., Wu Y. B., Chen F. K., and Jahn B. M. (2005) Zircon U–Pb age, element and C–O isotope geochemistry of post-collisional mafic–ultramafic rocks from the Dabie orogen in east-central China. *Lithos* **83**, 1–28.

Zheng Y. F., Fu B., Gong B., and Li L. (2003) Stable isotope geochemistry of ultrahigh pressure metamorphic rocks from the Dabie–Sulu orogen in China: implications for geodynamics and fluid regime. *Earth Sci. Rev.* **62**, 105–161.

*Associate editor:* Martin A. Menzies